

1 **Cloud [phase and macrophysical](#) properties over the Southern Ocean during**
2 **the MARCUS field campaign**

3

4 Baike Xi¹, Xiquan Dong¹, Xiaojian Zheng¹, and Peng Wu²

5

6 ¹Department of Hydrology and Atmospheric Sciences, University of Arizona, Tucson, AZ, USA

7 ²Pacific Northwest National Laboratory, Richland, WA, USA

8

9 **Correspondence:** Baike Xi (baikex@arizona.edu)

10

11

12

13

14

15

16

17

18

19

20

21

22

23

24 **Abstract.**

25 ___ To investigate the cloud [phase and macrophysical](#) properties over the Southern Ocean (SO), the
26 [Department of Energy \(DOE\) Atmospheric Radiation Measurement \(ARM\) Mobile Facility](#)
27 [\(AMF2\)](#) was installed on the Australian icebreaker *Aurora Australis* during the MARCUS field
28 campaign [41 to 69 °S; 60 to 160 °E] from October 2017 to March 2018. To examine cloud
29 properties over the mid-latitude and Polar regions, the study domain is separated into northern
30 (NSO) and southern (SSO) parts of the SO with a demarcation line of 60 °S. The total cloud
31 fractions (*CFs*) were 77.9 %, 67.6 %, and 90.3 % for the entire domain, NSO and SSO, respectively,
32 indicating that higher *CFs* were observed in the Polar region. Low-level clouds, [and](#) deep
33 [convective](#) clouds are the [two](#) most common cloud types over the SO.

34 [A new method was developed to classify liquid, mixed-phase and ice clouds in](#) single-layered
35 low-level clouds, [\(LOW\)](#) where mixed-phase clouds dominate with an occurrence frequency (*Freq*)
36 of 54.5 %, while the *Freq* of the liquid and ice clouds were 10.1 % (most drizzling) and 17.4 %
37 (least drizzling). The meridional distributions of low-level cloud boundaries are nearly
38 independent of latitude, whereas the cloud temperatures increased ~8 K and atmospheric
39 precipitable water vapor increased from ~5 mm at 69 °S to ~18 mm at 43 °S. The mean cloud liquid
40 water paths over NSO were much larger than those over SSO. Most liquid clouds occurred over
41 NSO with very few over SSO, whereas more mixed-phase clouds occurred over SSO than over
42 NSO. There were no significant differences for ice cloud *Freq* between NSO and SSO. [The ice](#)
43 [particle sizes are comparable to cloud droplets and drizzle drops, and well mixed in the cloud layer.](#)
44 These results will be valuable for advancing our understanding of the meridional and vertical
45 distributions of clouds and can be used to improve model simulations over the SO.

46

Deleted: (
Deleted:) was conducted
Deleted: , using ship-based measurements

Deleted: .

Deleted: cumulus, and shallow cumulus

Deleted: three

Deleted: For

Deleted: .

Deleted:

56 **1. Introduction**

57 The Southern Ocean (SO) is one of the cloudiest and stormiest regions on the Earth (Mace et
58 al., 2009; Chubb et al., 2013). Over the SO, most of the aerosols are naturally produced via oceanic
59 sources given the remote environment. The uncertainties of aerosol forcing caused by natural
60 emissions have larger variances than anthropogenic emissions, especially the dimethyl sulfide
61 (DMS) flux contributes significantly to the bias (Carslaw et al., 2013). The SO is a unique natural
62 laboratory to address the natural aerosol emissions and their contributions to the biases because it
63 has rich ecosystems and is remote to human activities (McCoy et al., 2015). However, we have
64 limited knowledge about cloud formation processes within such clean environments and their
65 associated aerosol and cloud properties. The unique nature of the SO region features low-level
66 supercooled liquid and mixed-phase clouds, which is significantly different from the subtropical
67 marine boundary layer (MBL) clouds where warm liquid clouds are dominant (Dong et al., 2014;
68 Wu et al., 2020; Zhao et al., 2020), and also different to the Arctic mixed-phase clouds which are
69 featured with the liquid-topped cloud layer with ice cloud layer beneath (Qiu et al., 2015).

Deleted: The majority

Deleted:).

70 Large biases in cloud amount and microphysics over the SO in the Coupled Model
71 Intercomparison Project phase 5 (CMIP5) climate models result in a near 30 W m^{-2} shortwave
72 radiation deficit at the top of the atmosphere (TOA) (Marchand et al., 2014; Stanfield et al., 2014,
73 2015), which further leads to unrealistic cloud feedbacks and equilibrium climate sensitivity (Bony
74 et al., 2015; Stocker et al., 2013). Meanwhile, the efficiency of aerosol-cloud interaction (ACI)
75 over the SO was found to be crucial for the models' sensitivities to the radiation budget. A new
76 aerosol scheme in the Hadley Centre Global Environmental model can dampen the ACI and
77 suppress negative clear-sky shortwave feedback, both of which contribute to a larger climate
78 sensitivity (Bodas-Salcedo et al., 2019).

81 A climate sensitivity study using CMIP6 general circulation models (GCMs) shows much
82 higher temperature variations across 27 GCMs in response to doubled CO₂ than those in CMIP5,
83 which may have resulted from the decreased extratropical low-level cloud cover and cloud albedo
84 over the SO in CMIP6 (Zelinka et al., 2020). Low-level clouds are a key climate uncertainty and
85 can explain 50 % of the inter-model variations (Klein et al., 2017) because conversion from liquid
86 cloud droplets to ice cloud particles decreases the cloud albedo and reduces the reflected shortwave
87 radiation at TOA. Models, however, have difficulties accurately partitioning the cloud phase
88 (Kalesse et al., 2016). The phase changes in mixed-phase clouds over the Arctic have proved to
89 affect the cloud lifetime and radiative properties significantly, that is, converting from ice cloud
90 particles to liquid cloud droplets may increase the cloud optical depth and the reflected shortwave
91 radiation at TOA (Morrison et al., 2012). In contrast, models that allow mixed-phase clouds to
92 glaciate rapidly can produce 30% more warming from doubling CO₂ (McCoy et al., 2014).

93 Phase transition processes have been investigated by several groups using both satellite and
94 ground-based measurements. [For instance, Mace and Protat \(2018\)](#) found that there are more
95 mixed-phase clouds over the SO measured from the ship than retrieved from CloudSat and
96 CALIPSO measurements because the satellites cannot accurately measure clouds below ~1 km.
97 [Lang et al. \(2018\)](#) used a model to investigate the clouds under post cold frontal systems and found
98 large biases in model simulations and concluded that the cloud cover and radiative biases over the
99 SO are highly regime dependent. Of all cloud types, low-level clouds are primarily responsible for
100 the biases in the model simulations due to the lack of reliable measurements, which leads to a poor
101 understanding of the conditions where these clouds form and the phase(s) that result. In other
102 words, a physical representation of clouds, especially for low-level clouds, is unclear but truly
103 necessary for improving model simulations. Therefore, reliable observations of the cloud macro-

Deleted: A study (

Deleted: ,

Deleted: A previous study (

Deleted: ..

108 and micro-physical properties from ground-based active and passive remote sensors are crucial for
109 the improvement of model simulations.

110 Previous studies show that cloud phase is primarily dependent on cloud temperature, and the
111 transition from one cloud phase to another will modify the cloud optical properties, which further
112 affects the radiation budgets (Hu et al., 2010; Intrieri et al., 2002; Morrison et al., 2012). Based on
113 satellite observations and retrievals, [Hu et al. \(2010\)](#) found that supercooled liquid water (SLW)
114 clouds are most common in the low-level clouds over the SO, where 80% of low-level clouds
115 contain SLW in a wide range of cloud temperatures from 0°C to -40°C. The formation of SLW
116 clouds is usually related to strong boundary layer convection. However, when ice nuclei exist in
117 the mixed-phase clouds, the ice particles can grow quickly and become bigger through consuming
118 supercooled liquid water drops. The SLW is inherently unstable due to the higher vapor pressure
119 over liquid than over ice and the quicker vapor deposition on ice particles than on liquid droplets
120 (Intrieri et al., 2002). As the supercooled liquid cloud droplets glaciate to ice particles, the cloud
121 layer becomes darker because the ice particles scatter less shortwave radiation and absorb more
122 radiation in the near IR wavelength regime. It is unclear, however, what role these ice particles
123 play in the low-level clouds over the SO, which includes the impact on drizzle development.

124 During HIAPER Pole-to-Pole Observation (HIPPO) campaigns, [Chubb et al. \(2013\)](#) found that
125 there are rarely ice particles in non-drizzling and light drizzling clouds over the SO, which may
126 imply that the ice particles in the mixed-phase clouds may modulate the drizzle formation.

127 To investigate the aerosol and cloud properties over the SO, a field campaign called the
128 Measurements of Aerosols, Radiation, and Clouds over the Southern Ocean (MARCUS) was
129 conducted using the ship-based measurements between Hobart, Australia, and the Antarctic during
130 the period October 2017-March 2018. The Department of Energy (DOE) Atmospheric Radiation

Deleted: they

Deleted: (Hu et al., 2010).

Deleted: the study in

134 Measurement (ARM) Mobile Facility (AMF2) was installed on the Australian icebreaker *Aurora*
135 *Australis*, which voyaged from Hobart, Tasmania to the Australian Antarctic stations of Casey,
136 Mawson, and Davis, as well as Macquarie Island as illustrated in Fig. 1. Another field campaign,
137 called South Ocean Clouds, Radiation, Aerosol Transport Experimental Study (SOCRATES) field
138 campaign was conducted during austral summer from January 15 to February 26, 2018. [In this](#)
139 [study, the aircraft](#) in-situ measurements [during SOCRATES are used](#) as [the](#) reference for [the](#)
140 analysis. The SOCRATES domain [is](#) shown [in the](#) black dotted rectangle box in Fig. 1. The
141 objectives of the MARCUS campaign are to investigate the vertical distribution of boundary layer
142 clouds and reveal the reasons why the mixed-phase clouds are common in the warm season
143 (McFarquhar et al., 2016; [McFarquhar et al., 2021](#)). [Our study will focus on cloud macrophysical](#)
144 [properties and cloud phase along the shiptracks during MARCUS.](#)

145 MARCUS ship-based instruments include AMF2 cloud radar, lidar, microwave radiometer,
146 micropulse lidar, radiosonde sounding, precision solar pyranometer and precision infrared
147 radiometer, as well as aerosol sensors. Through these comprehensive observations over the SO,
148 we are tentatively answering the following three scientific questions:

- 149 (1) What is the total cloud fraction over the SO during MARCUS, as well as vertical and
150 meridional variations in cloud fraction?
- 151 (2) What are the dominant cloud types over the SO, their associated cloud [phase and](#)
152 [macrophysical](#) properties, as well as their vertical and meridional distributions?
- 153 (3) What are the vertical and meridional distributions of the low-level clouds over the SO?

154 This manuscript is organized as follows: the data and method [and](#) introduced in section 2. The
155 statistical results for all clouds during MARCUS are summarized in section 3. The low-level cloud

Deleted: , which

Deleted: may use

Deleted: a

Deleted: this

Deleted: has

Deleted: as

Deleted:), which will be our focuses for this study.

Deleted: are

164 [phase and macrophysical](#) properties are described in section 4, followed by a summary and
165 conclusions in section 5.

166 **2. Data and Method**

167 **2.1 Ship-based measurements used in this study**

168 [The AMF2 instruments, measurements, and their corresponding uncertainties and references](#)

169 are [listed in Table 1](#). Because AMF2 was designed to support shipboard deployments, the [baseline](#)
170 [suite of instruments are marine-focused](#), including the 95-GHz W-band cloud radar, [\(WACR\)](#),

171 ceilometer, micropulse lidar, [\(MPL\)](#), microwave radiometer, [\(MWR\)](#), aerosol observation system
172 (AOS), meteorological measurements (MET, includes the following data: temperature, pressure,

173 specific humidity, wind direction, and speed) on the ship, rain gauge and the radiosonde soundings.

174 The combined cloud radar and ceilometer measurements can provide the cloud boundaries as long

175 as there are no optically thin clouds and the cloud-base heights (H_{base}) are not greater than the

176 upper limit (7.7 km) of the ceilometer. The micropulse lidar will be used to identify optically thin

177 clouds and the clouds with $H_{\text{base}} > 7.7$ km. A previous study has shown that these additional clouds

178 detected by the micropulse lidar can be a non-negligible supplement to the total cloud fraction

179 (Mace et al., 2021). [A detailed description of the instruments and the cloud parameters during](#)

180 [MARCUS can be found in Mace et al. \(2021\) and McFarquhar et al. \(2016 and 2021\)](#).

181 [In order to accurately estimate the cloud temperatures, we](#) adopted a linear interpolation

182 method based on [the daily balloon soundings \(4 to 5 times per day\)](#) to achieve a better temporal

183 resolution [of the vertical profiles](#) of temperature, pressure, and specific humidity. The method

184 considers MET measurements to ensure vertical continuity and adjacent soundings for temporal

185 continuity. Using these interpolated atmospheric profiles, cloud temperatures can be [obtained at a](#)

186 [5-min temporal resolution](#).

Deleted: ¶

Deleted: The cloud properties analyzed

Deleted: derived from

Deleted: data collected by AMF2

Deleted: .

Deleted: .

Deleted: .

Deleted: .

Deleted: There are about 4 to 5 radiosonde soundings per day. We...

Deleted: these

Deleted: accurately estimated.

199 The cloud liquid water path (*LWP*) and atmospheric precipitable water vapor (*PWV*) are
200 retrieved based on a physical-iterative algorithm using observations of the microwave radiometer
201 brightness [temperatures](#) at 23.8 and 31.4 GHz with uncertainties ranging from 15 to 30 g m⁻²
202 (Marchand et al., 2003). It is important to note that the brightness temperature biases switch signs
203 among different climatological regions because a threshold of 5 °C in cloud-base temperature was
204 used in their physical retrievals. [Since the retrieved LWP and PWV are based on the MWR](#)
205 [measured brightness temperatures at two frequencies, any biases on the brightness temperatures](#)
206 [will affect these retrievals. Therefore, we propose an extra step to determine the uncertainties](#)
207 [during MARCUS. Based on the temperature profiles, we can identify clouds that are not likely to](#)
208 [contain liquid \(e.g., pure ice-cloud\), then we can estimate the LWP uncertainty based on their](#)
209 [corresponding retrieved LWP values. From the probability density function \(PDF\) analysis, the](#)
210 [LWP uncertainty is estimated as 10 g m⁻² for MARCUS.](#)

211 [To determine the precipitation status](#), the AOS and rain gauge measurements were used to
212 determine whether rain is reaching the surface qualitatively, but not quantitatively in this study.
213 All the measurements were averaged over 5 minutes, except [the](#) radar reflectivity, Doppler velocity,
214 and spectrum width used in Section 4.3.

215 [2.2 Cloud type classification and single-layer low cloud phases](#)

216 A classification method [developed](#) in [Xi et al. \(2010\)](#) was used to categorize different types of
217 [clouds using ARM radar-lidar estimated cloud base \(\$H_{\text{base}}\$ \) and top \(\$H_{\text{top}}\$ \) heights and cloud](#)
218 [thickness \(\$\Delta H\$ \). A brief description of the classification of cloud types is as follows \(Table 1 and](#)
219 [Figure 6 in Xi et al., 2010\).](#) [The single-layered low-level clouds \(LOW\) is the fraction of time](#)
220 [when low clouds with \$H_{\text{top}} \leq 3\$ km occur without clouds above them. Middle clouds \(MID\) range](#)
221 [from 3 to 6 km without any clouds below and above, while high clouds \(HGH\) have \$H_{\text{base}} > 6\$ km](#)

Deleted: The cloud occurrence frequency can be determined through two steps: the column cloud fraction is simply the ratio of cloudy samples to the total observations in every 5-min; the occurrence frequency for each type of cloud during the entire time period equals the ratio of the number where column cloud fraction is greater than zero to the total 5-min samples.

Deleted: temperature

Deleted: Therefore, we propose an extra step to determine the uncertainties during MARCUS. Both

Deleted: The detailed

Deleted: will be introduced

Deleted: Section 4.1. In

Moved (insertion) [1]

235 with no cloud underneath. Other types of clouds are defined by different combinations of the above
236 three types, middle over low (MOL), high over low (HOL), high over middle (HOM), and the
237 cloud column through the entire troposphere is defined as HML. Three types, MOL, HOM, and
238 HML, include both contiguous and non-contiguous cloud layers, and their thicknesses may be
239 overestimated when clear layer(s) are present between any two cloud layers.

Moved (insertion) [2]

240 Furthermore, we used the measurements of interpolated sounding, microwave radiometer
241 retrieved *LWP*, radar reflectivity, Doppler velocity and spectrum width to classify the cloud phase
242 in each radar range volume of low-level clouds during MARCUS. The detailed classification
243 method will be introduced in Section 4.1. We also used ERA-Interim reanalysis data to study the
244 environmental conditions during MARCUS. The lower tropospheric stability (LTS) is calculated
245 from the potential temperature difference between the surface and 700 hPa to assess the boundary-
246 layer stabilities when the low-level clouds appeared along the shiptracks. The relative
247 contributions of mixed-phase, liquid and ice clouds to the single-layered low-level clouds as well
248 as their drizzling status are also analyzed in this study. The latitudinal and longitudinal variations
249 of the single-layered low-level clouds as well as their vertical distributions are further explored in
250 this study.

Deleted: ERA5

Deleted: and calculated the

Deleted: and estimated inversion strength (EIS)

Deleted: ¶

A classification method developed in Xi et al. (2010) was used to calculate the occurrence frequencies of different types of clouds and their corresponding cloud macrophysical properties, e.g., cloud base (H_{base}) and top (H_{top}) heights, cloud thickness ($ΔH$), and *LWP*.

Deleted: To further investigate the drizzling status under different cloud phases, we also calculated their LTS and EIS.

Deleted: also

251 3. Statistical results for all clouds during MARCUS

Deleted: ¶

252 The occurrence frequencies of total cloud cover and different types of clouds and their
253 associated properties over the entire study domain during MARCUS are presented in Figs. 2-4.
254 In order to examine the cloud properties over the mid-latitude and Polar regions, we separate the
255 SO domain into northern (NSO, north of 60°S) and southern (SSO, south of 60°S) parts using a
256 demarcation line of 60°S. A total of 2,447 hours cloud samples were collected during MARCUS
257 in this study, in which 1,181 hours of samples were located in the NSO and 1,266 hours of samples

Deleted: -

272 were collected from the SSO. It is important to note that adding micropulse lidar measurements
273 increased the total samples of non-liquid-containing clouds by ~20% because micropulse lidar is
274 more sensitive to optically thin clouds than cloud radar. However, micropulse lidar signals are
275 usually attenuated and cannot provide a meaningful signal when the liquid cloud layer is thicker
276 than a couple of hundred meters (Sassen, 1991).

277 Figure 2 shows the vertical distributions of total cloud cover over the entire domain, as well as
278 over NSO and SSO. For the vertical distributions, the occurrence frequencies of total cloud
279 increase from the first radar gate (~ 226 m) to ~700 m, then monotonically decrease with altitude
280 with a few small increments at different levels, especially over SSO. Comparing the occurrence
281 frequencies of total cloud between NSO and SSO, we can draw the following conclusions. 1) The
282 SSO has more cloudiness than the NSO under 7 km, while the NSO has more cloudiness than the
283 SSO above 7 km. 2) Below 3 km, the occurrence frequencies of clouds over the NSO decrease
284 dramatically from 37 % at an altitude of ~700 m to 16 % at 3 km and from 45 % to 28 % over the
285 SSO, which is similar to the vertical distributions of the low-level clouds over some Northern
286 Hemisphere mid-latitude regions, such as Eastern North Atlantic (ENA, Dong et al., 2014). The
287 occurrence frequencies measured during MARCUS are much lower than these shown in Fig. 8 of
288 Mace et al. (2009) throughout the entire vertical column between the same range of latitudes,
289 especially, the occurrence frequencies during MARCUS are almost half of those measured by
290 CloudSat and CALIPSO from 1 to 3 km. The reason has been explained in Xi et al. (2010), that
291 is, a comparison of occurrence frequencies between measurements of two different platforms can
292 only be performed under an equivalent spatial-to-temporal resolution. In other words, our results
293 were calculated under 5-min temporal resolution, and the results in Mace et al. (2009) were
294 statistically in the 2° gridbox. Therefore, the comparison between these two results is not

Deleted: We can draw the following conclusions by comparing...

Deleted: the

Deleted: .

Deleted: these

Deleted: .

Deleted: .

Deleted: 2 ° grid box

303 reasonable. To make a fair comparison, one has to know the cloud amount at each area or time
304 step, then the product of amount and frequency is independent of either temporal and spatial
305 measurement.

306 To compare with other studies, we calculated the cloud fractions (*CFs*) of total and different
307 types of clouds. The total *CFs* were 77.9 %, 67.6 %, and 90.3 % for the entire domain, NSO and
308 SSO, respectively, indicating that 22.7 % more clouds occurred in the Polar region than in the mid-
309 latitude region. The total *CF* over the entire domain is very close to the 76 % calculated by Mace
310 and Protat (2018) using ship-based measurements during the Cloud, Aerosols, Precipitation,
311 Radiation and Atmospheric Composition (CAPRICORN) field experiment. The total *CF* over the
312 SSO is close to that estimated by using the complementarity of CALIOP lidar aboard CALIPSO
313 and CPR aboard CloudSat (DARDAR version 2 data) from Listowski et al. (2019).

314 [Figure 3](#) shows the occurrence frequencies of categorized clouds and their cloud boundaries
315 using the maximum H_{top} and the minimum H_{base} [if there are two or more layers in each 5-min](#)
316 [sample. For example, the mean \$H_{base}\$ and \$H_{top}\$ for single-layered low-level \(LOW\) are 0.92 km and](#)
317 [1.62 km, respectively, listed in Table 2, which are the average values of min \$H_{base}\$ and max \$H_{top}\$ in](#)
318 [LOW category.](#) As illustrated in Fig. 3a, the single-layered low-level (LOW), deep cumulus or
319 multi-layered (HML), and MOL clouds are the three dominant types of clouds over the SO.
320 Comparing the clouds between NSO and SSO, all types of clouds in SSO [have higher frequency](#)
321 [of occurrence](#) than those in NSO except HOL. The differences range from less than 1 % (LOW)
322 to more than 10 % (MOL). Comparing the clouds over mid-latitude oceans between the two
323 hemispheres, i.e., between NSO and ARM ENA site (Dong et al., 2014), we find: (1) The total
324 cloud fractions (*CFs*) are close to each other (67.6 % over NSO vs. 70.1 % at ARM ENA); (2)
325 LOW *CFs* are 22.9 % vs. 27.1 %, which is the dominant type of cloud in both regions; and (3)

Deleted: very

Deleted: Figure

Deleted: . The definition of each type of cloud follows the method of Xi et al. (2010). A brief description of the classification of cloud types is as follows.

Moved up [1]: The single-layered low-level clouds (LOW) is the fraction of time when low clouds with $H_{top} \leq 3$ km occur without clouds above them. Middle clouds (MID) range from 3 to 6 km without any clouds below and above, while high clouds (HGH) have $H_{base} > 6$ km with no cloud underneath. Other types of clouds are defined by different combinations of the above three types, middle over low (MOL), high over low (HOL), high over

Deleted: mid (HOM), and the cloud column through the entire troposphere is defined as HML.

Moved up [2]: Three types, MOL, HOM, and HML, include both contiguous and non-contiguous cloud layers, and their thicknesses may be overestimated when clear layer(s) are present between any two cloud layers.

Deleted: ¶

Deleted: shallow cumulus (

Deleted:)

Deleted: are

349 Both MOL and HML clouds, including underneath low clouds, are 14.2 % and 16.5 % over NSO,
350 much higher than those (4.2 % and 12.1 %) at ARM ENA site, indicating that there are more MOL
351 and deep convective clouds over NSO than over ENA.

352 Figure 3b shows the vertical locations of different types of cloud layers, which represent the
353 mean H_{top} and H_{base} listed in Table 2 for any type of cloud. Nearly all H_{top} and cloud thickness (ΔH)
354 values over NSO are higher or deeper than those over SSO, presumably due to stronger solar
355 radiation and stronger convection over NSO. H_{base} values basically followed their cloud-top
356 counterparts with a couple of exceptions. These cloud macrophysical properties are closely
357 associated with large-scale dynamic patterns and environmental conditions. By analyzing the
358 ERA-Interim reanalysis (not shown), the 850 hPa geopotential heights show persistent westerlies
359 with slightly higher geopotential heights over the northwest corner of the domain, which may
360 closely relate to the higher H_{top} over NSO than over SSO. Furthermore, the boundary layer over
361 NSO is relatively more stable than over SSO based on lower troposphere stability (LTS analysis
362 (12.2-15.32 K over NSO vs. 11.48-13.29 K over SSO)).

363 When we plot the probability density functions (PDFs) of cloud $LWPs$ for different types of
364 clouds, we find that the PDFs of $LWPs$ for HGH and HOM peak are less than 10 g m^{-2} . These
365 results make physical sense because HGH clouds should not contain any liquid droplets, and most
366 HOM clouds, especially those over SSO, should be ice phase dominant. In addition, the 10 g m^{-2}
367 of LWP is close to the uncertainty of the LWP retrieval in Marchand et al., (2003). Therefore, this
368 value is used as a threshold for all types of clouds, which leads to less than one percent reduction
369 of the total samples. As shown in Fig. 4a, the $LWPs$ ($> 10 \text{ g m}^{-2}$) for all types of clouds are much
370 higher over NSO than over SSO because the low-level and MOL clouds in the mid-latitudes
371 contain more liquid water than those in Polar regions. The mean $LWPs$ for liquid containing low-

Deleted: shallow

Deleted: maximum

Deleted: minimum

Deleted: , as well as their deepest ΔH

Deleted: ΔH

Deleted: I

Deleted: analysis.

Deleted: at

Deleted: .

Deleted: shallow convective

382 level and middle-level clouds over NSO, i.e. LOW, MID and HOL, range from ~130 to 150 g m⁻²,
383 while the mean *LWPs* for MOL and HML are two times higher (~270 g m⁻²) than the mean *LWP*
384 of LOW, MID and HOL. Note that the mean *LWPs* for most types of clouds over the SSO are
385 much lower than those over the NSO, except for the LOW clouds.

386 The occurrence frequencies of *LWPs* (> 10 g m⁻²) over NSO and SSO contradict their cloud
387 *LWP values* as demonstrated in Fig. 4b. To further investigate the amount of available precipitable
388 water vapor (*PWV*), we found that mean *PWV* values in SSO are at least 2 to 3 times less than
389 those in NSO for same types of clouds (figure not shown). Note that the samples of MID, HGH,
390 and HOM clouds are excluded from this study when they have *LWPs* less than 10 g m⁻², since
391 these low *LWPs* are within the retrieval uncertainty of cloud *LWP* and hence may not contain any
392 liquid cloud droplets. The higher *LWPs*, larger cloud droplets, drizzle drops and ice particles, and
393 greater drizzling occurrence frequencies over NSO (which is discussed later) will lead to the quick
394 dissipation of clouds over NSO. In contrast to NSO, the SSO cloud *LWPs* and particle sizes are
395 much smaller with less drizzling events, which increases cloud lifetime relative to NSO. The 67.6 %
396 and 90.3 % *CFs* over NSO and SSO provide strong evidence for this argument. We can draw the
397 following conclusions by comparing the cloud macrophysical properties between NSO and SSO
398 in Figs. 3 and 4. The LOW fraction, thickness, and *LWP* over NSO and SSO are comparable to
399 each other. For other types of clouds, cloud thicknesses are similar to each other or slightly deeper
400 over NSO, but the cloud *LWPs* over NSO are much larger than those over SSO, resulting in more
401 precipitation events over NSO. As pointed out in Albrecht (1989), more precipitation events may
402 reduce the cloud lifetime. This argument is consistent with the results shown in Figs. 2 and 3a for
403 all clouds except for HOL. Cloud lifetimes over NSO are shorter than those over SSO, which leads
404 to lower *CFs* over NSO than over SSO.

Deleted: such as

Deleted: shallow and deep convective clouds, such as

Deleted: ,

Deleted: Table 1 provides a summary of the average, standard derivation, minimum and maximum for cloud boundaries, liquid water path and the percentage of multi-layered cloud for each cloud type over the SO. Non-contiguous...

Moved down [3]: clouds over the SO occur very frequently, especially for HOM and HML. The *LWP* for single-layered clouds is greater than that for multi-layered clouds. The *LWP* for single-layered HML almost doubles that for multi-layered HML.¶

Deleted: counterparts,

Deleted: the

Deleted: fewer

Deleted: (

422 Table 2 provides a summary of the mean, standard derivation, minimum and maximum for
423 cloud boundaries, LWP and the percentage of multi-layered cloud for each cloud type over the SO.
424 Non-contiguous (multi-layer) clouds over the SO occur very frequently, especially for HOM and
425 HML. The LWP for single-layered clouds is greater than that for multi-layered clouds. The LWP
426 for single-layered HML almost doubles that for multi-layered HML.

Deleted: ¶

Moved (insertion) [3]

427 **4. Single-layered low-level clouds**

428 As discussed in Section 3, single-layered low-level clouds (LOW) are the dominant cloud type
429 in both northern (NSO) and southern (SSO) parts of the SO. Figs. 3 and 4 further reveal that LOW
430 cloud type is the only one having comparable *CF*, cloud, thickness, *LWP* over both NSO and SSO.
431 This warrants further study: Are the cloud phases, properties, and vertical and meridional
432 variations of LOW clouds over these two regions similar to each other or significantly different?

433 **4.1. Cloud phase**

434 In this study, cloud boundaries are determined by combining cloud radar, ceilometer and
435 micropulse lidar measurements at a temporal resolution of 5-min. The cloud phase, liquid water
436 droplets or ice particles, are determined in each radar range volume. A flow chart for classifying
437 the phases of single-layered low-level clouds is drawn in Fig. 5. The determination of warm liquid
438 clouds is straightforward using both cloud-base (T_{base}) and -top (T_{top}) temperatures greater than 0
439 °C, and cloud *LWPs* greater than the threshold (10 g m^{-2}). The determination of supercooled liquid
440 clouds is slightly complicated. When either T_{base} or T_{top} is below 0° C , and cloud *LWPs* are greater
441 than the threshold, the radar Doppler spectrum width (*WID*) and velocity (V_d) are used for the
442 determination of supercooled liquid water clouds. If the majority (10 seconds of original radar
443 measurements) of *WID* within a 5-min period are less than 0.4 m s^{-1} and V_d are equal to or less than
444 0.0 m s^{-1} (updrafts) in the volume, then this range volume is defined as supercooled liquid clouds.

446 Mixed-phase clouds are determined when the [median](#) (calculated from 10 seconds of original
447 radar measurements) of *WID* is greater than 0.4 m s^{-1} [or](#) V_d is greater than 0.0 m s^{-1} (downdrafts)
448 due to the existence of large ice particles in the clouds. If cloud *LWP* is below the threshold, then
449 it is defined as an ice cloud, otherwise, it is defined as a mixed-phase cloud. It is worth mentioning
450 that large ice particles, which grow through vapor deposition or rime processes, dominate the radar
451 reflectivity and are heavier than cloud droplets. Therefore, these large ice particles not only
452 broaden the spectrum width but also have relatively large fall speeds.

453 To further evaluate our classification method, we compared the classified mixed-phase and ice
454 clouds with the micropulse lidar linear depolarization ratios (*LDR*) as an extra measure. The *LDR*
455 ranges follow the method in Shupe et al., (2005), which are $0.11 < LDR < 0.15$ for mixed-phase
456 clouds, and $LDR > 0.15$ for ice clouds, [as listed in Table 1. Table 3a](#) shows the quantitative
457 comparison of the cloud phase identifications between these two classification methods. The
458 numbers represent the counts of each matched 5-min sample, where the diagonal numbers indicate
459 that both methods are identifying the same type of cloud phase. In general, the two methods have
460 89 % agreement on the phase identification. Secondly, we performed the phase classification
461 directly from microphysical probes onboard G-1 aircraft during SOCRATES and treated them as
462 'ground-truth' (Mohrmann et al., 2021). [Since the in-situ cloud microphysical measurements can](#)
463 [tell us the phase of the cloud, it allows us to see the percentage variations of cloud phase, by](#)
464 [changing integration time of in-situ sampling to mimic what the radar may observe the cloud for](#)
465 [each range volume, Table 3b](#) shows [possible cloud phase partitionings](#) that may be detected by
466 cloud radar. As sampling time increases from 1 second to 30 seconds, more mixed-phase clouds
467 and fewer single-phase clouds can be observed.

Deleted: medians

Deleted: and

Deleted: .

Deleted: .

Deleted: .

Deleted: 2a

Deleted: By

Deleted: the

Deleted: step

Deleted: .

Deleted: 2b

Deleted: the statistics of the possibility of the

480 Figure 6 shows the determination of mixed-phase and ice clouds through combined
 481 measurements of radar reflectivity and spectrum width, lidar LDR and backscatter, and cloud LWP.
 482 For the classified ice clouds, cloud LWPs are lower than 10 gm⁻² (Fig. 6f), most of the Doppler
 483 spectrum widths range from 0.08 to 0.16 m s⁻¹ (Fig. 6b) and the LDR ratios (Fig. 6d) can be greater
 484 than ~0.15, representing a narrow range of ice particle size distribution with higher LDR ratios.
 485 For the classified mixed-phase clouds, cloud LWPs are greater than 10 gm⁻² and most of the
 486 Doppler spectrum widths range from 0.15 to 0.5 m s⁻¹, representing a broad particle size
 487 distribution resulting from the mixture of liquid droplets and ice particles. An interesting result
 488 occurs where both LDR signals (>0.2) and LWPs are much higher during the drizzling periods
 489 (Fig. 6a), indicating a mixed-phase cloud with cloud droplets within the cloud layer and large
 490 liquid drizzle drops and ice crystals below cloud base.

491 Based on the Doppler velocity, the mode values for both mixed-phase and ice clouds occur at
 492 ~ 0.5 m s⁻¹, where the ice particles are dominant in both types of clouds. The broader particle size
 493 distribution with lower LDR ratios for mixed-phase clouds and narrower particle size distribution
 494 with higher LDR ratios for ice clouds further corroborate that the classified results from this study
 495 are consistent with the traditional micropulse lidar LDR method.

496 It is important to note that the micropulse lidar signals are usually attenuated and cannot
 497 provide a meaningful signal when the liquid cloud layer is thicker than a couple of hundred meters
 498 (Sassen, 1991). Arctic mixed-phase clouds are typical, with the liquid-dominant layer on the top of
 499 the mixed-phase clouds and the ice-dominant layer underneath. The ceilometer-derived cloud-base
 500 height represents the base of the liquid-dominant layer near the cloud top, while MPL-derived
 501 cloud-base height represents the base of the lower ice-dominant layer (Qiu et al., 2015; Shupe,
 502 2007; Shupe et al., 2005). Over the Arctic, the micropulse lidar signals can penetrate through the

Deleted: occurrence frequencies

Deleted: the matched results for

Deleted: clouds (left panel)

Deleted: (right column).

Deleted: up to

Deleted: 5

Deleted: Cloud liquid is identified by low LDR of ~0.11 (Fig. 6d) and high lidar backscatter from 10⁻⁵ to 10⁻⁴ m⁻¹ sr⁻¹ (Fig. 6e).

Deleted: width

Deleted: 35

Deleted: and most of the LDR signals are less than 0.4

Deleted: but lower LDR ratios.

Deleted: .

517 ice-dominant layer to the liquid-dominant layer. However, the mixed-phase clouds over the
518 Southern Ocean are totally different from those over the Arctic region: they are well mixed (liquid
519 droplets and ice particles) from cloud base to cloud top, which is found in this study. Thus, the
520 micropulse lidar signals can be attenuated in the mixed-phase clouds over the Southern Ocean.
521 Statistical results show that 43 % of micropulse [lidar signals](#) were attenuated during MARCUS
522 compared to our classified results.

Deleted: data

523 This classification method is further supported by the onboard cloud radar measurements
524 during the Southern Ocean Clouds Radiation Aerosol Transport Experimental Study (SOCRATES,
525 not shown). In that campaign, the reflectivity measurements were usually greater, and the spectrum
526 widths were much wider when the aircraft observed large ice particles compared to the time
527 periods when liquid cloud droplets were observed. [Although the wider spectrum widths might be
528 caused by Doppler broadening of the moving aircraft, further analysis shows that the onboard radar
529 sends the signals \(assuming the time of transmitted and received signals is short enough comparing
530 to aircraft speed\) in the perpendicular to the movement of the aircraft, that is, there is no relative
531 movement between radar signals and clouds. Thus, the onboard radar spectrum width
532 measurements should be not significantly impacted by Doppler broadening \(relative movement in
533 the same direction\).](#)

534 [In this study, a total of 6,934 5-min single-layered low-level cloud samples were determined
535 using our classificaiton method, including 697 liquid cloud samples, 3,777 mixed, 1,205 ice, and
536 1,255 'OTHER' clouds. ~~The category of 'OTHER' clouds represents more than one phase in each~~
537 \[column.\]\(#\) Note that though the 'OTHER' is also mixed-phase cloud, it has different vertical
538 \[distribution of liquid compared to the 'mixed' cloud.\]\(#\) It is also worth mentioning that about 5.5 %](#)

Moved (insertion) [4]

540 of single-layered low-level cloud phases cannot be determined when the radar measurements were
541 not available during MARCUS, those were not accounted to "OTHER".

542 Figure 7 (upper panel) shows the drizzling status for each categorized cloud type, i.e., no rain
543 (yellow-green), virga (brown) and rain (navy blue). The definition of drizzling status follows the
544 method in Wu et al., (2015, 2017) where there are radar reflectivity measurements below the
545 ceilometer/lidar determined cloud base. The major difference for drizzles in the studies of Wu et
546 al. (2015, 2017) and this study is that drizzle is liquid phase at ARM ENA site but could be both
547 liquid and ice phases in this study.

548 The percentages shown below the x-axis represent the portion of drizzling status in each type
549 of clouds, such as liquid, mixed-phase, ice and 'OTHER' clouds. Figure 7 (bottom panel) also
550 shows the percentages and vertical distributions of classified liquid, mixed-phase, ice, and
551 'OTHER' clouds for each column in the single-layered low-level clouds, represented by different
552 colors. After classification, the samples in each category are sorted by their H_{top} . In detail, Figure
553 7 demonstrates that the mixed-phase clouds dominate the single-layered low-level cloud category
554 with an occurrence frequency of 54.5 %. The 'OTHER' and ice clouds have similar occurrence
555 frequencies of 18.1 % and 17.4 %, respectively, while the liquid clouds have the lowest occurrence
556 frequency of 10.1 %. The liquid-topped mixed-phase clouds (included in 'OTHER'), which
557 frequently occur in the Arctic region (Qiu et al., 2015), are rarely found over the SO. The existence
558 of ice particles in mixed-phase clouds should strongly depend on the distribution of ice nuclei (IN),
559 whereas spatially unevenly distributed IN may result in the OTHER type of clouds.

560 Based on the results in Fig. 7, we draw the following conclusions. Most of the ice clouds are
561 without icy precipitation, and the percentages with virga and precipitation below the cloud base
562 are 12 % and 15 %, respectively. The percentages of non-drizzling, virga and drizzling mixed-

Deleted: . Therefore, using our classification method, a total of 6,934 5-min single-layered low-level cloud samples were determined in this study, including 697 liquid cloud samples, 3,777 mixed, 1,205 ice, and 1,255 'OTHER' clouds.

Moved up [4]: The category of 'OTHER' clouds represents more than one phase in each column.

Deleted: .g

Deleted:), which used both ceilometer and cloud radar measurements to determine the status of MBL clouds under non-drizzling, virga and rain conditions.

Deleted: Fig.

Deleted: least

Deleted:

Deleted: non-drizzling clouds

Deleted: drizzle

578 phase clouds are 50 %, 21 %, and 29 %. The liquid and 'OTHER' clouds have similar percentages,
579 they are 36 %, 25 % and 39 % for liquid clouds, and 35 %, 22 % and 44 % for 'OTHER' clouds.
580 For liquid and 'OTHER' clouds, the drizzling frequencies are independent of H_{top} . In contrast, for
581 mixed-phase and ice clouds, the drizzling frequencies strongly depend on H_{top} , i.e., higher drizzling
582 frequencies occur mostly at higher H_{top} .

583 The properties of single-layered low-level clouds are summarized in Table 4. The liquid clouds
584 have the lowest H_{base} and H_{top} but more available water vapor than other types of clouds. Since the
585 'OTHER' clouds are a transitional stage among mixed-phase, liquid and ice clouds, they have the
586 highest H_{top} , deepest cloud layer and largest LWP . The ice clouds occur in relatively dry
587 environments and have the highest H_{base} at 1.218 km, and thinnest cloud layer. The cloud variables
588 for mixed-phase clouds fall between Liquid and "OTHER". Since $LWPs$ in mixed-phase clouds
589 have larger standard deviation, which implies that SLW is more common at higher $LWPs$ and ice
590 is more common at lower $LWPs$.

591 4.2. Meridional variations of cloud properties

592 Figure 8 shows the meridional variation in single-layered low-level cloud properties during
593 MARCUS. As illustrated in Fig. 8a, the meridional distributions of H_{base} , H_{top} and ΔH are nearly
594 independent of latitude, however, their corresponding temperatures (T_{base} and T_{top}) increased about
595 8 K from 69 °S to 43 °S, though there were slight fluctuations. These results suggest that the cloud
596 and sea surface temperatures have minimal impact on the cloud boundaries over the SO, which is
597 consistent with the findings in McFarquhar et al. (2016). The meridional variation of $LWPs$ follows
598 those of T_{base} and T_{top} , with an increasing trend from south to north. It is important to point out that
599 a big drop in LWP at ~50 °S results from fewer occurrences of low-level clouds there, indicating
600 that the cloud samples at some latitudes are not statistically significant. The atmospheric PWV

Deleted: 3

Deleted: .

Deleted: have similar H_{base} , but lower H_{top} , LWP and PWV compared to those of 'OTHER' clouds.

Deleted: deviations

Deleted: mimics

607 increased dramatically from ~ 5 mm at 69 °S to ~18 mm at 43 °S, presumably due to increased sea
608 surface and atmospheric temperatures.

609 Figure 9 shows the latitudinal and meridional distributions of categorized liquid, mixed-phase,
610 ice and 'OTHER' in single-layered low-level clouds over the SO during MARCUS. Each circle
611 represents the exact location and time along the ship track. Mixed-phase clouds occurred
612 everywhere over the SO during the MARCUS field campaign and became dominant in November,
613 December and February. Liquid clouds dominated in March, while ice clouds dominated in
614 January. The 'OTHER' clouds are a kind of transitional phase falling in between the mixed-phase
615 and ice/liquid clouds because there are no stand-alone occurrences in any month during MARCUS.

616 **4.3 Vertical distribution of cloud properties**

617 The vertical distributions of classified liquid, mixed-phase, and ice clouds [in LOW category](#)
618 are presented in Figs. 10-12. The focus of this section will be comparisons of cloud [macrophysical](#)
619 properties between the north (NSO) and south (SSO) regions of the domain. Figure 10a shows the
620 vertical distributions of liquid clouds, which were capped at ~ 1.6 km, mostly in the marine
621 boundary layer. The vertical occurrence frequencies are up to 27 % over NSO, while they were
622 less than 4 % over SSO, i.e., liquid clouds occurred fairly often over the mid-latitude region, but
623 very few occurred over the Polar region. On the contrary, the occurrence frequencies of mixed-
624 phase clouds between NSO and SSO are opposite to liquid clouds, as illustrated in Fig. 10b, though
625 the differences are not so obvious. Mixed-phase clouds increased with altitude until ~1.6 km, then
626 decreased monotonically towards 3 km. The highest frequencies were ~37 % at 0.6 km over SSO
627 and ~27 % at 1.5 km over NSO. The vertical distributions of ice clouds are similar to those of
628 mixed-phase clouds (Fig. 10c), [however](#), there were no significant differences between NSO and
629 SSO. It is worth mentioning that the vertical distributions of mixed-phased clouds over SO are

Deleted: .

Deleted:). However

632 quite different to those from DOE ARM Northern Slope Alaska (NSA) site, where the [low-level](#)
633 mixed-phase clouds are [commonly featured with a liquid-topped layer](#). (e.g., Qiu et al., 2015).

Deleted: liquid topped

Deleted: low-level

Deleted: common

634 To further investigate the vertical distributions of classified liquid, mixed-phase, and ice clouds
635 over NSO and SSO, we plot the normalized vertical distributions (cloud base as 0, cloud top as 1)
636 of radar reflectivity, Doppler velocity and spectrum width in Figs. 11 and 12, respectively. In this
637 study, the threshold of -50 dBZ was used to determine the cloud boundary over the SO instead of
638 the threshold of -40 dBZ radar reflectivity used at the ARM ENA site (Dong et al., 2014). If we
639 used the threshold of -40 dBZ over the SO, then there would be only 73% cloud samples available,
640 [If we used the threshold of -50 dBZ, then we would have 90.4% cloud samples, which gained](#)
641 [additional 17.4% on top of the -40 dBZ threshold](#). About 9.6% of radar reflectivities during
642 MARCUS are [lower](#) than -50 dBZ for all [LOW](#) cloud samples, [but without ceilometer and MPL](#)
643 [lidar signals](#). Thus [these 9.6% cloud samples were eliminated in Figs 11-12](#).

Deleted:

Deleted: for this study.

Deleted:

Deleted: less

Deleted: dBz

Deleted: single-layered low-level

Deleted: all radar parameters used

Deleted: this study are based on 90.4 % of the radar measurements with reflectivity greater than -50 dBz.

644 Figures 11a-11c represent the normalized vertical distributions of radar reflectivity, Doppler
645 velocity and spectrum width of liquid clouds. Liquid clouds had the lowest reflectivity near the
646 cloud top because of cloud-top entrainment., The reflectivity had a nearly constant median value
647 of ~ -22 dBZ from [cloud top height](#) (~ 0.8 for normalized height) of the cloud layer to the cloud
648 base. Most of the reflectivities were less than -15 dBZ, which is [a](#) threshold to distinguish cloud
649 [droplets](#) and drizzle, [drops](#) in each radar range volume (Wu et al., 2020). Most of the Doppler
650 velocities were greater than 0.0 m s⁻¹, indicating that downwelling motion is dominant in liquid
651 clouds. The profiles of Doppler velocity and spectrum width increased smoothly from the cloud
652 top to base, suggesting that larger cloud droplets and broader size distributions exist near the cloud
653 base, which is attributable to more drizzle drops near the cloud base, as illustrated in Fig. 7.

Deleted: near

Deleted: dBz

Deleted: the

Deleted: -sized particles

Deleted: .

671 The vertical distributions of mixed-phase clouds in Figs. 11d-11f are similar to those of liquid
672 clouds. The more occurrences of larger reflectivity measurements and larger median values of
673 spectrum width near the cloud base are most likely due to the presence of moderate ice particles
674 and/or drizzle drops. The nearly same median values of reflectivity, Doppler velocity and spectrum
675 width (but slightly larger standard deviations in each level in mixed-phase clouds) in both liquid
676 and mixed-phase clouds suggest that the ice particle sizes in mixed-phase clouds are comparable
677 to cloud droplets and drizzle drops. The nearly uniform vertical distributions of Doppler velocity
678 and spectrum width indicate well-mixed liquid cloud droplets and ice particles throughout the
679 cloud layer in the mixed-phase clouds over NSO.

680 Compared to liquid and mixed-phase clouds, ice clouds had much lower reflectivities and
681 narrower spectrum width as shown in Figs. 11g-11i. Almost all reflectivity measurements were
682 less than -25 dBz with a median value of -35 dBz at the cloud base, resulting from small or
683 moderate ice particles but much lower concentration. A nearly constant Doppler velocity within
684 the cloud layer further supports the discussion of mixed-phase clouds above, i.e., the ice particle
685 sizes are independent of cloud height and comparable to liquid cloud droplets in the low-level
686 clouds over the SO. Because there are no mechanisms for growing large ice particles in such
687 shallow ice clouds, the accretion process cannot take place. From the statistical results in Fig. 7,
688 these ice particles have relatively little chance to become virga or raindrops and usually dissipate
689 or transition to other types of clouds.

690 Since there are not enough liquid cloud samples over the Polar region, only the mixed-phase
691 and ice clouds results are shown in Fig. 12. Compared to the vertical distributions of ice clouds
692 over NSO, the median values of reflectivity and Doppler spectrum width over SSO were lower
693 and narrower, indicating a lack of large ice particles in the Polar region. The small ice particles in

Deleted: Ice

Deleted: reflectivity

Deleted: than liquid and mixed-phase clouds,

Deleted: plotted

698 the Polar region were also reflected in their mixed-phase clouds. Compared to the vertical
699 distributions of the mixed-phased clouds over NSO, the median values of reflectivity and Doppler
700 spectrum width over SSO were dramatically lower (-35 dBz at SSO vs. -22 dBz at NSO; 0.25 m
701 s^{-1} at SSO vs. 0.32 $m s^{-1}$ at NSO). Figure 12 illustrates that the ice particle sizes over SSO are
702 smaller, their size distributions are narrower than those over NSO, [indicative](#) of lack of large ice
703 particles over SSO.

Deleted: indicating

704 5. Summary and Conclusions

Deleted: ¶

705 In this study, we presented the statistical results of clouds over the Southern Ocean (SO), and
706 [its](#) northern (NSO) and southern (SSO) parts during MARCUS [Intensive observational period](#)
707 [\(IOP\)](#). We used the method developed in Xi et al., (2010) to calculate the occurrence frequencies
708 of different types of clouds and their corresponding cloud macrophysical properties. We developed
709 a new method to classify liquid, mixed-phased, and ice clouds in the single-layered low-level
710 clouds as well as their corresponding drizzling status. Lastly, we explored the meridional and
711 vertical distributions of these classified cloud properties. Analysis of the MARCUS cloud [phase](#)
712 [and macrophysical](#) properties has yielded the following conclusions.

Deleted:)

Deleted: the

Deleted: .

Deleted: .

713 1) The total cloud fractions (*CFs*) were 77.9 %, 67.6 %, and 90.3 % for the entire domain, NSO
714 and SSO, respectively, indicating that 22.7 % more clouds occurred in the Polar region than in
715 the mid-latitude region. The SSO had more clouds under 7 km, while the NSO had more clouds
716 above 7 km. Below 3 km, the occurrence frequencies of clouds over NSO decrease
717 dramatically from 37 % at an altitude of [~0.7 km](#) to 16 % at 3 km, which is similar to the
718 vertical distributions of the low-level clouds over some Northern Hemisphere mid-latitude
719 regions, such as Eastern North Atlantic.

Deleted: 700 m

727 2) The single-layered low-level (LOW), deep [connective](#) or multi-layered (HML), and [MOL](#),
728 clouds are the three dominant types of clouds over the SO. Comparing the clouds between
729 NSO and SSO, all types of clouds in SSO are higher than those in NSO except HOL. The LOW
730 fraction, thickness, LWP over both NSO and SSO are comparable to each other. The mean
731 LWPs for [LOW, MID and HOL](#) clouds over NSO, range from ~130 to 150 g m⁻², while the
732 mean [NSO LWPs \(~270 g m⁻²\)](#) for [MOL](#) and deep convective clouds, [\(HML\)](#) are two times
733 higher than the same types of clouds [over SSO](#). The mean LWPs of clouds over SSO are much
734 lower than the LWPs over NSO. Over the Southern Ocean, the single-layered or contiguous
735 clouds usually have higher [LWP](#) than their [counterparts](#) of multi-layered or non-contiguous
736 clouds. There are more non-contiguous HML and HOM than contiguous ones.

737 3) A new method was developed to classify liquid, mixed-phase and ice clouds in the single-
738 layered low-level clouds (LOW) based on comprehensive ground-based observations. The
739 mixed-phase clouds are dominant in the [LOW](#) cloud category with an occurrence frequency of
740 54.5 %. The 'OTHER' and ice clouds had similar occurrence frequencies of 18.1 % and 17.4 %,
741 respectively, while the liquid clouds had the least occurrence frequency of 10.1 %. The
742 percentages of non-drizzling, virga and drizzling for mixed-phase clouds were 50 %, 21 %,
743 and 29 %, and the drizzling frequencies of mixed-phase clouds strongly depend on H_{top} , that
744 is, higher drizzling frequencies occurred mostly at higher H_{top} .

745 4) The meridional distributions of H_{base} , H_{top} and ΔH are nearly independent on latitude, [however](#),
746 their corresponding temperatures increased about 8 K from 69 °S to 43 °S. The meridional
747 variation of LWPs mimics that of cloud temperatures, having an increasing trend from south
748 to north. The mean PWV increased dramatically from ~ 5 mm at 69 °S to ~18 mm at 43 °S due
749 to increased sea surface and atmospheric temperatures. More liquid clouds occurred over NSO

Deleted: cumulus

Deleted: shallow cumulus (

Deleted:)

Deleted: low

Deleted: such as LOW, MOL and HOL,

Deleted: shallow

Deleted: , such as MOL and

Deleted: ,

Deleted: (~270 g m⁻²)

Deleted: liquid water paths

Deleted: counterpart

Deleted: single-layered low-level

Deleted: . However

763 but very few occurred over SSO, whereas more mixed-phase clouds occurred over SSO than
764 over NSO. There were no significant differences in ice clouds occurrences between NSO and
765 SSO.

766 5) The nearly same median values of reflectivity, Doppler velocity and spectrum width in both
767 liquid and mixed-phase clouds over NSO suggest that the ice particle sizes in mixed-phase
768 clouds are comparable to cloud droplets and drizzle drops. The uniform vertical distributions
769 of Doppler velocity and spectrum width suggest well-mixed liquid cloud droplets and ice
770 particles throughout the cloud layer in the mixed-phase clouds over NSO, which are quite
771 different from those over the DOE ARM NSA site where the liquid-topped mixed-phase low-
772 level clouds are common. The median values of reflectivity and Doppler spectrum width over
773 SSO were lower and narrower than those over NSO, indicating lack of large ice particles in
774 the polar region.

775 These results provide comprehensive statistical properties of all clouds over the SO during
776 MARCUS, including the occurrence frequencies of different types of clouds and their
777 corresponding cloud macrophysical properties. We also examined the meridional and vertical
778 distributions of the classified cloud properties. These statistics can be used as a ground truth to
779 evaluate satellite retrieved cloud properties and model simulations over the SO. The results of this
780 study will help to advance our understanding of the clouds over the SO, which may lead to
781 improved model simulations, as well as better representation of global climate.

782

Deleted:

Deleted:

Deleted: these

Deleted: over the SO

Deleted: a

Deleted: ¶

789 *Data availability.* Data used in this study can be accessed from the DOE [ARM's Data Discovery](https://adc.arm.gov/discovery/) at
790 <https://adc.arm.gov/discovery/>

Deleted: ARM's

791
792 *Author contributions.* The idea of this study is discussed by BX, XD, and XZ. BX and XZ performed
793 the analyses and BX wrote the manuscript. BX, XD, XZ and PW participated in scientific discussions
794 and provided substantial comments and edits on the paper.

795
796 *Competing interests.* The authors declare that they have no conflict of interest.

797
798 *Acknowledgements.* The ground-based measurements were obtained from the Atmospheric
799 Radiation Measurement (ARM) Program sponsored by the U.S. Department of Energy (DOE)
800 Office of Energy Research, Office of Health and Environmental Research, and Environmental
801 Sciences Division. The data can be downloaded from <http://www.archive.arm.gov/>. Researchers
802 were supported by the NSF project under grant AGS-2031750 at the University of Arizona.
803 Specially thanks to Mr. Xingyu Zhang for providing analysis from CDP and 2DS microphysical
804 sensors during SOCRATES and Dr. Dale Ward for proofreading this manuscript.

Deleted: at the University of Arizona

805

Deleted: ¶
¶
¶

811 **References.**

- 812 Albrecht, B. A.: Aerosols, cloud microphysics, and fractional cloudiness, *Science*,
813 doi:10.1126/science.245.4923.1227, 1989.
- 814 Bodas-Salcedo, A., Mulcahy, J. P., Andrews, T., Williams, K. D., Ringer, M. A., Field, P. R. and
815 Elsaesser, G. S.: Strong Dependence of Atmospheric Feedbacks on Mixed-Phase
816 Microphysics and Aerosol-Cloud Interactions in HadGEM3, *J. Adv. Model. Earth Syst.*,
817 doi:10.1029/2019MS001688, 2019.
- 818 Bony, S., Stevens, B., Frierson, D. M. W., Jakob, C., Kageyama, M., Pincus, R., Shepherd, T. G.,
819 Sherwood, S. C., Siebesma, A. P., Sobel, A. H., Watanabe, M. and Webb, M. J.: Clouds,
820 circulation and climate sensitivity, *Nat. Geosci.*, doi:10.1038/ngeo2398, 2015.
- 821 Chubb, T. H., Jensen, J. B., Siems, S. T. and Manton, M. J.: In situ observations of supercooled
822 liquid clouds over the Southern Ocean during the HIAPER Pole-to-Pole Observation
823 campaigns, *Geophys. Res. Lett.*, doi:10.1002/grl.50986, 2013.
- 824 Dong, X., Xi, B., Kennedy, A., Minnis, P. and Wood, R.: A 19-month record of marine aerosol-
825 cloud-radiation properties derived from DOE ARM mobile facility deployment at the
826 Azores. Part I: Cloud fraction and single-layered MBL cloud properties, *J. Clim.*,
827 doi:10.1175/JCLI-D-13-00553.1, 2014.
- 828 Hu, Y., Rodier, S., Xu, K. M., Sun, W., Huang, J., Lin, B., Zhai, P. and Josset, D.: Occurrence,
829 liquid water content, and fraction of supercooled water clouds from combined
830 CALIOP/IIR/MODIS measurements, *J. Geophys. Res. Atmos.*,
831 doi:10.1029/2009JD012384, 2010.

832 Intrieri, J. M., Fairall, C. W., Shupe, M. D., Persson, P. O. G., Andreas, E. L., Guest, P. S. and
833 Moritz, R. E.: An annual cycle of Arctic surface cloud forcing at SHEBA, *J. Geophys. Res.*
834 *Ocean.*, doi:10.1029/2000jc000439, 2002.

835 Klein, S. A., Hall, A., Norris, J. R. and Pincus, R.: Low-Cloud Feedbacks from Cloud-Controlling
836 Factors: A Review, *Surv. Geophys.*, doi:10.1007/s10712-017-9433-3, 2017.

837 Kalesse, H., de Boer, G., Solomon, A., Oue, M., Ahlgrimm, M., Zhang, D., Shupe, M. D., Luke,
838 E. and Protat, A.: Understanding rapid changes in phase partitioning between cloud liquid
839 and ice in stratiform mixed-phase clouds: An arctic case study, *Mon. Weather Rev.*,
840 doi:10.1175/MWR-D-16-0155.1, 2016.

841 Lang, F., Huang, Y., Siems, S. T. and Manton, M. J.: Characteristics of the Marine Atmospheric
842 Boundary Layer Over the Southern Ocean in Response to the Synoptic Forcing, *J. Geophys.*
843 *Res. Atmos.*, doi:10.1029/2018JD028700, 2018.

844 Listowski, C., Delanoë, J., Kirchgaessner, A., Lachlan-Cope, T. and King, J.: Antarctic clouds,
845 supercooled liquid water and mixed phase, investigated with DARDAR: Geographical and
846 seasonal variations, *Atmos. Chem. Phys.*, doi:10.5194/acp-19-6771-2019, 2019.

847 Mace, G. G., Zhang, Q., Vaughan, M., Marchand, R., Stephens, G., Trepte, C. and Winker, D.: A
848 description of hydrometeor layer occurrence statistics derived from the first year of merged
849 Cloudsat and CALIPSO data, *J. Geophys. Res. Atmos.*, doi:10.1029/2007JD009755, 2009.

850 Mace, G. G. J. and Protat, A.: Clouds over the Southern Ocean as observed from the R/V
851 investigator during CAPRICORN. Part I: Cloud occurrence and phase partitioning, *J. Appl.*
852 *Meteorol. Climatol.*, doi:10.1175/JAMC-D-17-0194.1, 2018.

853 Mace, G. G., Protat, A., Humphries, R. S., Alexander, S. P., McRobert, I. M., Ward, J., Selleck,
854 P., Keywood, M. and McFarquhar, G. M.: Southern Ocean Cloud Properties Derived From

855 CAPRICORN and MARCUS Data, J. Geophys. Res. Atmos., doi:10.1029/2020JD033368,
856 2021.

857 Marchand, R., Ackerman, T., Westwater, E. R., Clough, S. A., Cady-Pereira, K. and Liljegren, J.
858 C.: An assessment of microwave absorption models and retrievals of cloud liquid water
859 using clear-sky data, J. Geophys. Res. Atmos., doi:10.1029/2003jd003843, 2003.

860 Marchand, R., Wood, R., Bretherton, C., McFarquhar, G., Protat, A., Quinn, P., Siems, S., Jakob,
861 C., Alexander, S., Weller, B.: The Southern Ocean Clouds, Radiation Aerosol Transport
862 Experimental Study (SOCRATES), whitepaper available from
863 [http://www.atmos.washington.edu/socrates/SOCRATES_white_paper_Final_Sep29_201](http://www.atmos.washington.edu/socrates/SOCRATES_white_paper_Final_Sep29_2014.pdf)
864 [4.pdf](http://www.atmos.washington.edu/socrates/SOCRATES_white_paper_Final_Sep29_2014.pdf), 2014.

865 McCoy, D. T., Hartmann, D. L. and Grosvenor, D. P.: Observed Southern Ocean cloud properties
866 and shortwave reflection. Part II: Phase changes and low cloud feedback, J. Clim.,
867 doi:10.1175/JCLI-D-14-00288.1, 2014.

868 McFarquhar, G., Bretherton, C., Alexander, S., DeMott, P., Marchand, R., Protat, A., Quinn, P.,
869 Siems, S., Weller, R., Wood, R.: Measurements of Aerosols, Radiation, and Clouds over
870 Sothern Ocean (MARCUS) Science Plan, DOE ARM Climate Research Facility.,
871 DOE/SC-ARM-16-011, available at: [http://arm.gov/publications/programdocs/doe-sc-](http://arm.gov/publications/programdocs/doe-sc-arm-16-011.pdf)
872 [arm-16-011.pdf](http://arm.gov/publications/programdocs/doe-sc-arm-16-011.pdf), 2016.

873 [McFarquhar, G. M., Bretherton, C. S., Marchand, R., Protat, A., DeMott, P. J., Alexander, S. P.,](#)
874 [Roberts, G. C., Twohy, C. H., Toohey, D., Siems, S., Huang, Y., Wood, R., Rauber, R. M.,](#)
875 [Lasher-Trapp, S., Jensen, J., Stith, J. L., Mace, J., Um, J., Järvinen, E., Schnaiter, M.,](#)
876 [Gettelman, A., Sanchez, K. J., McCluskey, C. S., Russell, L. M., McCoy, I. L., Atlas, R.](#)
877 [L., Bardeen, C. G., Moore, K. A., Hill, T. C. J., Humphries, R. S., Keywood, M. D.,](#)

878 [Ristovski, Z., Cravigan, L., Schofield, R., Fairall, C., Mallet, M. D., Kreidenweis, S. M.,](#)
879 [Rainwater, B., D'Alessandro, J., Wang, Y., Wu, W., Saliba, G., Levin, E. J. T., Ding, S.,](#)
880 [Lang, F., Truong, S. C. H., Wolff, C., Haggerty, J., Harvey, M. J., Klekociuk, A. R., and](#)
881 [McDonald, A.: Observations of Clouds, Aerosols, Precipitation, and Surface Radiation](#)
882 [over the Southern Ocean: An Overview of CAPRICORN, MARCUS, MICRE, and](#)
883 [SOCRATES, B. Am. Meteorol. Soc., 102, E894-E928, 10.1175/BAMS-D-20-0132.1,](#)
884 [2021.](#)

885 Mohrmann, J., Finlon, J., Atlas, R., Lu, J., Hsiao, I., Wood, R.: University of Washington Ice-
886 Liquid Discriminator single particle phase classifications and 1 Hz particle size
887 distributions/heterogeneity estimate, Version 1.0. UCAR/NCAR - Earth Observing
888 Laboratory., doi:10.26023/PA5W-4DRX-W50A, Last Access: Nov 01, 2021

889 Morrison, H., De Boer, G., Feingold, G., Harrington, J., Shupe, M. D. and Sulia, K.: Resilience of
890 persistent Arctic mixed-phase clouds, Nat. Geosci., doi:10.1038/ngeo1332, 2012.

891 [Muradyan, P. and Coulter, R.: Micropulse Lidar \(MPL\) Instrument Handbook. DOE ARM Climate](#)
892 [Research Facility, DOE/SC-ARM-TR-019, 2020. Available at:](#)
893 https://www.arm.gov/publications/tech_reports/handbooks/mpl_handbook.pdf, last access:
894 [25 March 2022.](#)

895 Qiu, S., Dong, X., Xi, B. and Li, J. L. F.: Characterizing Arctic mixed-phase cloud structure and
896 its relationship with humidity and temperature inversion using ARM NSA observations, J.
897 Geophys. Res., doi:10.1002/2014JD023022, 2015.

898 [Rémillard, J., Kollias, P., Luke, E., and Wood, R.: Marine Boundary Layer Cloud Observations in](#)
899 [the Azores, J. Climate, 25, 7381-7398, 10.1175/JCLI-D-11-00610.1, 2012.](#)

900 Sassen, K.: The polarization lidar technique for cloud research: a review and current assessment,
901 Bull. - Am. Meteorol. Soc., doi:10.1175/1520-0477(1991)072<1848:TPLTFC>2.0.CO;2,
902 1991.

903 Shupe, M. D., Uttal, T. and Matrosov, S. Y.: Arctic cloud microphysics retrievals from surface-
904 based remote sensors at SHEBA, J. Appl. Meteorol., doi:10.1175/JAM2297.1, 2005.

905 Shupe, M.: A ground-based multisensory cloud phase classifier, Geophys. Res. Lett.,
906 doi:10.1029/2007GL031008, 2007.

907 Stanfield, R. E., Dong, X., Xi, B., Kennedy, A., Del Genio, A. D., Minnis, P. and Jiang, J. H.:
908 Assessment of NASA GISS CMIP5 and Post-CMIP5 Simulated Clouds and TOA
909 Radiation Budgets Using Satellite Observations. Part I: Cloud Fraction and Properties, J.
910 Clim., doi:10.1175/jcli-d-13-00558.1, 2014.

911 Stanfield, R. E., Dong, X., Xi, B., Del Genio, A. D., Minnis, P., Doelling, D. and Loeb, N.:
912 Assessment of NASA GISS CMIP5 and post-CMIP5 simulated clouds and TOA radiation
913 budgets using satellite observations. Part II: TOA radiation budget and CREs, J. Clim.,
914 doi:10.1175/JCLI-D-14-00249.1, 2015.

915 Stocker, T. F., Qin, D., Plattner, G. K., Tignor, M. M. B., Allen, S. K., Boschung, J., Nauels, A.,
916 Xia, Y., Bex, V. and Midgley, P. M.: Climate change 2013 the physical science basis:
917 Working Group I contribution to the fifth assessment report of the intergovernmental panel
918 on climate change., 2013.

919 [Toto, T. and Jensen, M.: Interpolated Sounding and Gridded Sounding Value-Added Products.](#)
920 [DOE ARM Climate Research Facility, DOE/SC-ARM-TR-183, 2016. Available at:](#)
921 https://www.arm.gov/publications/tech_reports/doe-sc-arm-tr-183.pdf, last access: 25
922 [March 2022.](#)

923 [Uin, J.: Cloud Condensation Nuclei Particle Counter Instrument Handbook. DOE ARM Climate](#)
924 [Research Facility, DOE/SC-ARM-TR-168, 2016. Available at:](#)
925 https://www.arm.gov/publications/tech_reports/handbooks/ccn_handbook.pdf, last access:
926 [25 March 2022.](#)

927 Wu, P., Dong, X. and Xi, B.: Marine boundary layer drizzle properties and their impact on cloud
928 property retrieval, *Atmos. Meas. Tech.*, doi:10.5194/amt-8-3555-2015, 2015.

929 Wu, P., Dong, X., Xi, B., Liu, Y., Thieman, M. and Minnis, P.: Effects of environment forcing on
930 marine boundary layer cloud-drizzle processes, *J. Geophys. Res.*,
931 doi:10.1002/2016JD026326, 2017.

932 Wu, P., Dong, X. and Xi, B.: A climatology of marine boundary layer cloud and drizzle properties
933 derived from ground-based observations over the azores, *J. Clim.*, doi:10.1175/JCLI-D-20-
934 0272.1, 2020.

935 Xi, B., Dong, X., Minnis, P. and Khaiyer, M. M.: A 10 year climatology of cloud fraction and
936 vertical distribution derived from both surface and GOES observations over the DOE ARM
937 SPG site, *J. Geophys. Res. Atmos.*, doi:10.1029/2009JD012800, 2010.

938 Zelinka, M. D., Myers, T. A., McCoy, D. T., Po-Chedley, S., Caldwell, P. M., Ceppi, P., Klein, S.
939 A. and Taylor, K. E.: Causes of Higher Climate Sensitivity in CMIP6 Models, *Geophys.*
940 *Res. Lett.*, doi:10.1029/2019GL085782, 2020.

941 Zhao, L., Zhao, C., Wang, Y., Wang, Y. and Yang, Y.: Evaluation of Cloud Microphysical
942 Properties Derived From MODIS and Himawari-8 Using In Situ Aircraft Measurements
943 Over the Southern Ocean, *Earth Sp. Sci.*, doi:10.1029/2020EA001137, 2020.

Deleted: ¶

944
945

Table 1. ARM AMF2 instruments and their corresponding measurements and uncertainties used in this study

Deleted: Minimum cloud

<u>Parameter</u>	<u>Instruments/ Methods</u>	<u>Uncertainty</u>	<u>References</u>
<u>Cloud-base height</u>	<u>Ceilometer/MPL</u>	<u>15 m</u>	<u>Rémillard et al., 2012</u>
<u>Cloud-top height</u>	<u>95 GHz cloud radar</u>	<u>43 m</u>	<u>Rémillard et al., 2012</u>
<u>Cloud-base and -top temps</u>	<u>Radiosonde sounding</u>	<u>0.2 °C</u>	<u>Toto and Jensen, 2016</u>
<u>Profiles of reflectivity, Doppler velocity and Spectra</u>	<u>W-band ARM Cloud Radar (WACR), 95 GHz</u>	<u>Sensitivity: -50 dBZ at 2 km</u>	<u>Rémillard et al., 2012</u>
<u>linear depolarization ratios (LDR) and backscatter</u>	<u>Micropulse lidar, MPL</u> <u>Liquid: LDR<0.11</u> <u>Mix: 0.11<LDR<0.15</u> <u>Ice: LDR> 0.15</u>		<u>Shupe et al. 2005</u> <u>Muradyan and Coulter, 2020</u>
<u>Cloud LWP</u>	<u>Microwave radiometer</u>	<u>~15-30 g m⁻²</u> <u>Physical retrieval</u>	<u>Marchand et al., 2003</u>
<u>CCN and aerosol properties</u>	<u>Aerosol Observing System</u>	<u>1-min resolution;</u> <u>Uncertainties < 10%</u>	<u>Uin, 2016</u>

Table 2. Mean, standard deviation, minimum and maximum cloud-base heights (H_{base}), -top heights (H_{top}), and $LWPs$ (all samples, single-layered, multilayered) of all seven types of clouds over the **SO. All cloud heights have a unit of kilometer, and LWP has a unit of $g\ m^{-2}$.**

	LOW	MID	MOL	HGH	HOM	HML	HOL
$H_{base} \pm std$	0.92 ± 0.57	4.14 ± 0.61	1.37 ± 0.96	8.51 ± 2.23	4.70 ± 0.80	1.22 ± 0.98	1.14 ± 0.57
min, max	0.06, 2.86	3.00, 5.84	0.06, 5.27	6.00, 18.67	3.01, 7.72	0.06, 7.81	0.07, 10.57
$H_{top} \pm std$	1.62 ± 0.63	4.88 ± 0.68	4.29 ± 0.89	9.75 ± 2.13	7.93 ± 1.27	7.81 ± 1.35	8.93 ± 1.66
min, max	0.29, 3.0	3.17, 6.0	1.39, 5.99	6.20, 18.79	5.47, 17.98	3.62, 17.38	1.79, 17.56
$LWP \pm std$	122.4 ± 134.2	86.7 ± 124.5	168.7 ± 236.7	/	40.9 ± 40.8	169.2 ± 238.4	$129.8 \pm 202.$
Max LWP	1470.8	501.1	1937.1	/	345.7	1819.3	1785.2
$LWP \pm std$ (single layer) max	126.6 ± 138.1 1470.8	88.7 ± 128.9 501.1	193.1 ± 271.9 1937.1	/ /	48.7 ± 51.7 345.7	270.8 ± 349.5 1819.3	/ /
$LWP \pm std$ (multi-layer) max	96.2 ± 103.4 842.3	77.2 ± 109.2 305.6	139.0 ± 180.7 1830.2	/ /	32.3 ± 21.3 86.8	148.4 ± 202.4 1690.7	$129.8 \pm 202.$ 1785.2
Multi-layer percentage %	18.1	39.6	50.0	44.9	73.1	77.7	100

* The definition of the cloud types as follow: LOW (H_{base} and $H_{top} \leq 3\ km$); MID ($H_{base} > 3\ km$ and $H_{top} \leq 6\ km$); HGH ($H_{base} > 6\ km$); MOL ($H_{base} < 3\ km$ and $H_{top} \leq 6\ km$); HOM ($3\ km < H_{base} < 6\ km$ and $H_{top} > 6\ km$); HML ($H_{base} < 3\ km$, $H_{top} \geq 6\ km$ with a MID layer); HOL (LOW and HGH appear at the same time).

Deleted: maximum cloud

Deleted: liquid water paths (

Deleted:)

Deleted: Southern Ocean. Cloud

Deleted: .

Deleted: ¶

Table 3a. Comparison of cloud phase identifications between our classification method and Shupe et al. (2005) method in each 5-min measurements, the unit is number of 5-min samples.

Shupe this study	Liquid (this study)	Mixed-phase (this study)	Ice (this study)
Liquid	468	490	0
Mixed-phase	98	3840	0
Ice	81	0	1195

*Numbers denote the cloud sample classifications between two methods. For example, the number 98 denote a total of 98 samples are classified as Mixed-phase using Shupe's method, while are classified as Liquid using this study's method.

Table 3b. The cloud phase partitioning from CDP and 2DS during SOCRATES

Phase partitioning	1 second	10 seconds	30 seconds
Samples #	27,280	2,255	836
Liquid, %	58.8	26.2	18.8
Mixed-phase, %	38.9	69.1	77.0
Ice, %	2.3	4.7	4.2

Note that Cloud Droplet Probe (CDP) measures particle size from 2 to 50 um in diameter; Two-Dimensional Stereo Probe (2DS) measures particle size from 50 to 5000 um in diameter.

Deleted: 2a

Deleted: .

Deleted: /

Deleted: Shupe's

Deleted: study's

Deleted: ¶

¶

¶

Deleted: 2b

Moved (insertion) [5]

Deleted: .

Deleted: Phase partitioning

Moved up [5]: Liquid, %

Deleted: ¶

¶

¶

¶

¶

¶

¶

¶

¶

¶

¶

¶

¶

¶

¶

¶

¶

¶

¶

¶

¶

¶

¶

¶

¶

¶

¶

¶

¶

¶

¶

¶

¶

¶

Table 4. Liquid, mixed, ice and OTHER phases of cloud properties within the single-layered low-level clouds

Phase	Samples	H_{base} , km	H_{top} , km	ΔH , km	LWP , g m ⁻²	PWV , mm
Liquid	697	0.424±0.204	1.327±0.242	0.903	113.6±90.1	15.7±3.5
Mixed	3777	0.834±0.465	1.434±0.617	0.587	119.7±136.6	8.9±5.0
Ice	1205	1.218±0.635	1.737±0.651	0.519	0	8.4±4.5
OTHER	1255	0.700±0.454	1.774±0.571	1.074	141.9±137.5	11.4±5.9

Deleted: 3

Deleted: ¶

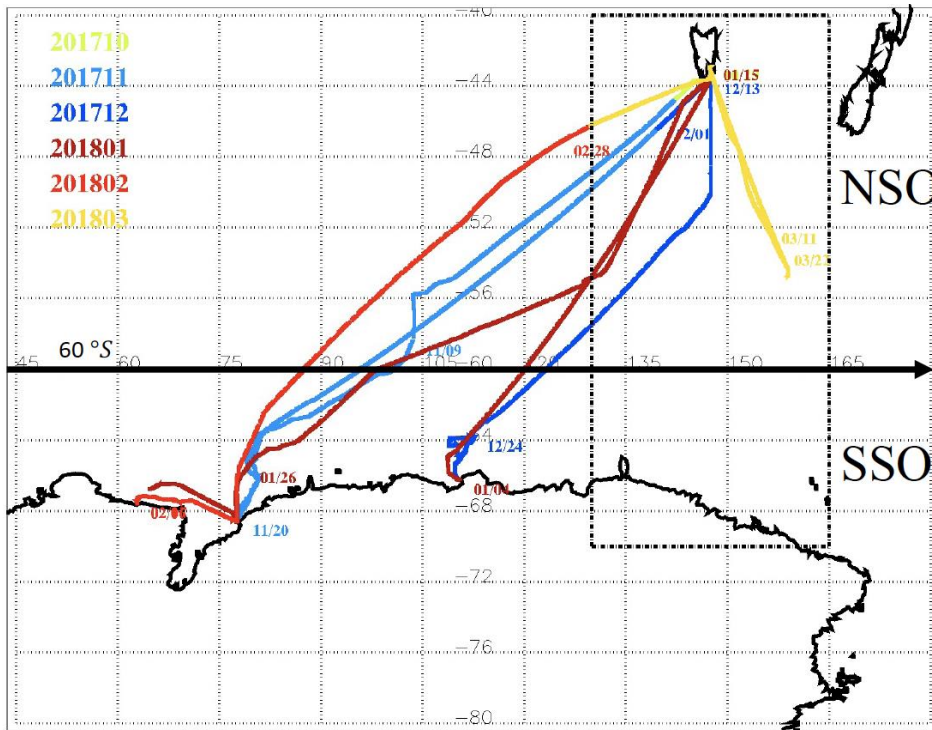


Figure 1. Shiptrack measurements between Hobart, Australia and Antarctica. Different colors represent different month's shiptracks from Oct. 29, 2017 to Mar. 23, 2018 during MARCUS. Along the shiptracks, the study domain is separated into northern (NSO) and southern (SSO) parts of the Southern Ocean with a demarcation line of 60 °S in order to study the clouds over the mid-latitudes (North of 60 °S) and Polar region (South of 60 °S). The black dotted rectangle represents the SOCRATES study domain. Some of the dates are labeled along the shiptracks, indicating the direction of the ship.

Deleted: ¶

Deleted: have

Deleted: which can indicate

Deleted: traveled

Deleted: ¶



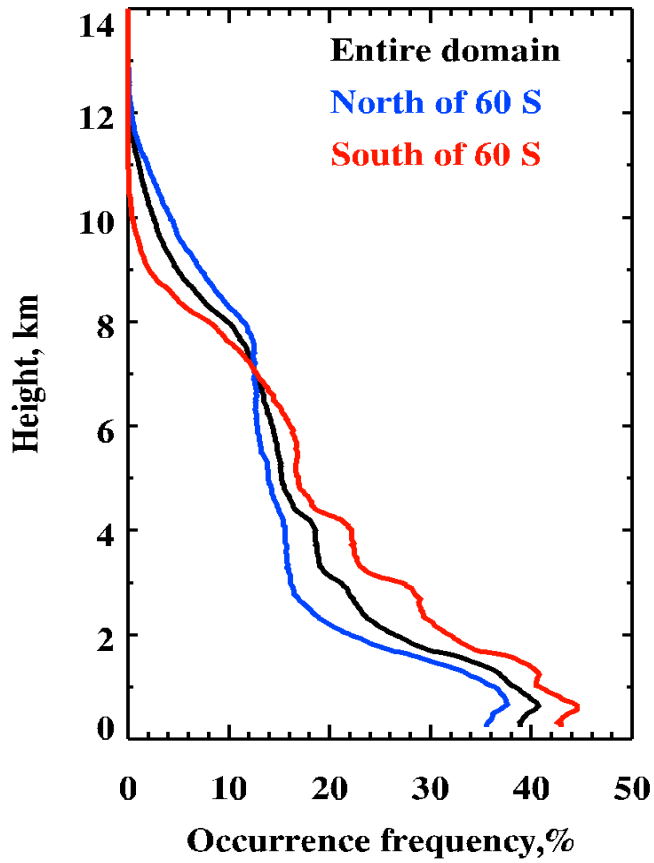
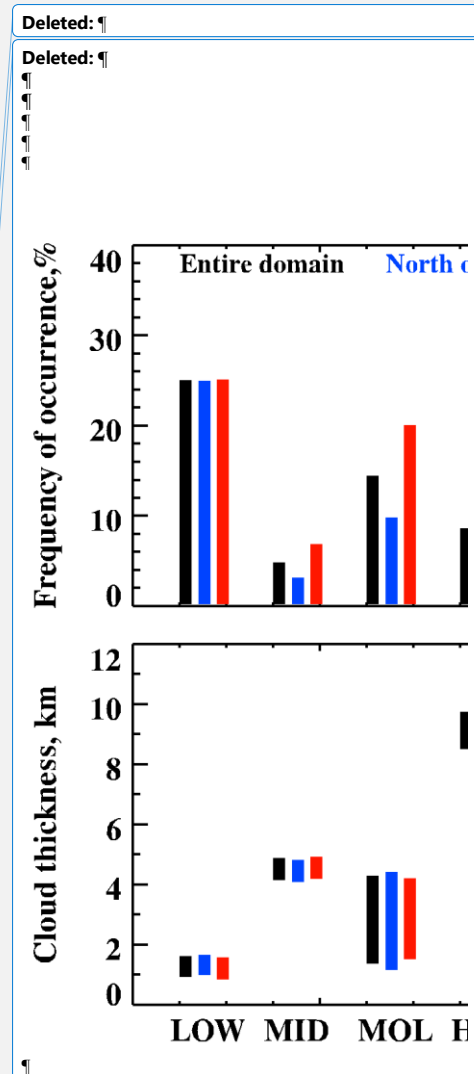


Figure 2. Mean vertical distributions of total clouds derived from ARM radar-lidar observations with a 5-min temporal resolution and a 30-m vertical resolution during MARCUS.



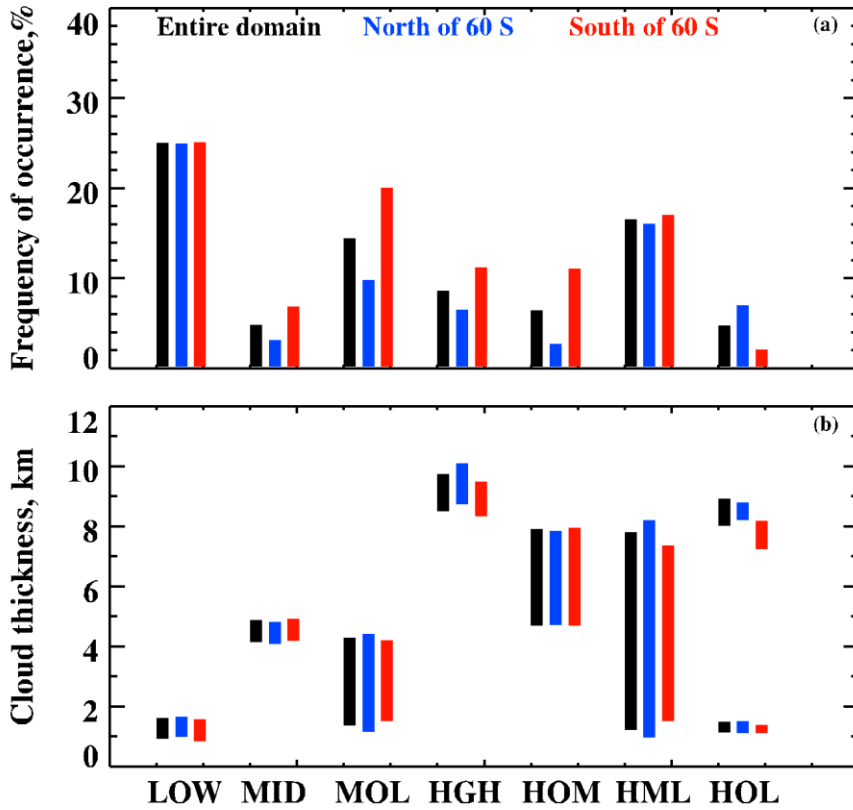
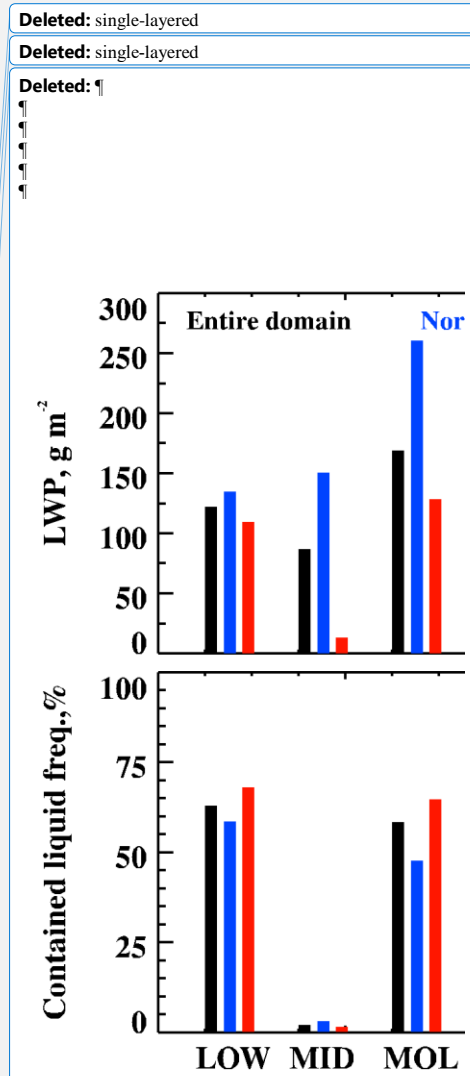


Figure 3. (a) Occurrence frequencies of categorized clouds by their vertical structures. LOW, single-layered low clouds (H_{base} and $H_{\text{top}} \leq 3 \text{ km}$); MID, singlelayered middle clouds ($H_{\text{base}} > 3 \text{ km}$ and $H_{\text{top}} \leq 6 \text{ km}$); MOL, MID over LOW ($H_{\text{base}} < 3 \text{ km}$ and $H_{\text{top}} \leq 6 \text{ km}$); HGH, singlelayered high clouds ($H_{\text{base}} > 6 \text{ km}$); HOM, HGH over MID ($3 \text{ km} < H_{\text{base}} < 6 \text{ km}$ and $H_{\text{top}} > 6 \text{ km}$); HML, HGH over MID and LOW ($H_{\text{base}} < 3 \text{ km}$, $H_{\text{top}} \geq 6 \text{ km}$ with a MID layer); and HOL, HGH over LOW (LOW and HGH appear at the same time). (b) Cloud thickness for each type of clouds (bar), the top and bottom of the bar represent the maximum cloud-top and minimum cloud-base heights, respectively. Black, blue, and red bars represent the entire domain (Lat:41-69 °S; Long: 60-160° E), north of 60 °S (NSO), and south of 60°S (SSO), respectively, during the MARCUS field campaign (10/2017-3/2018).



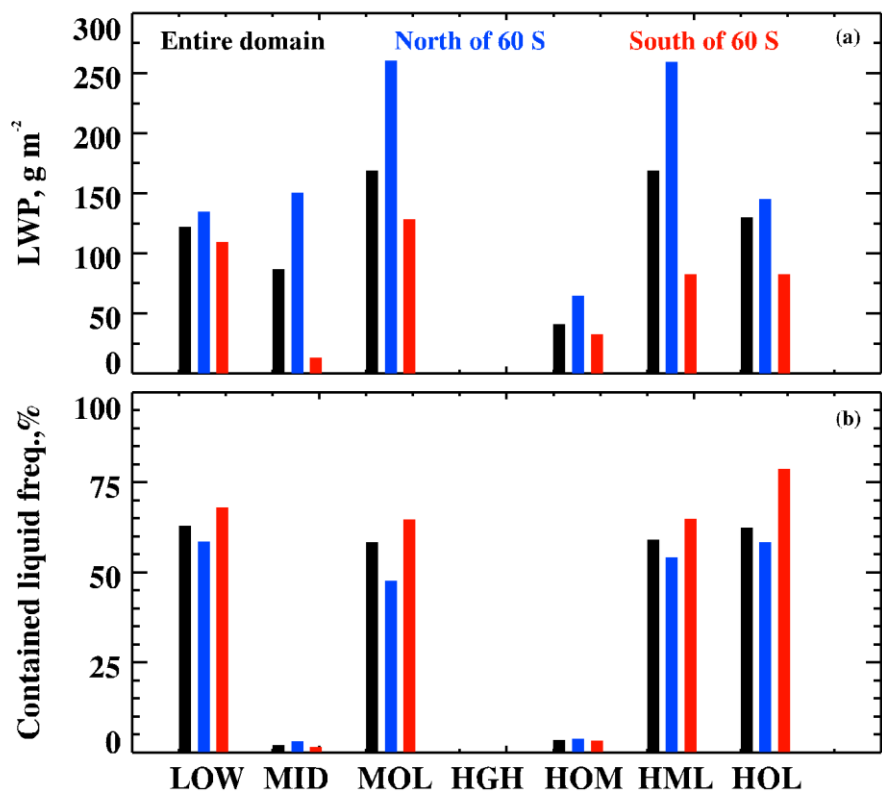
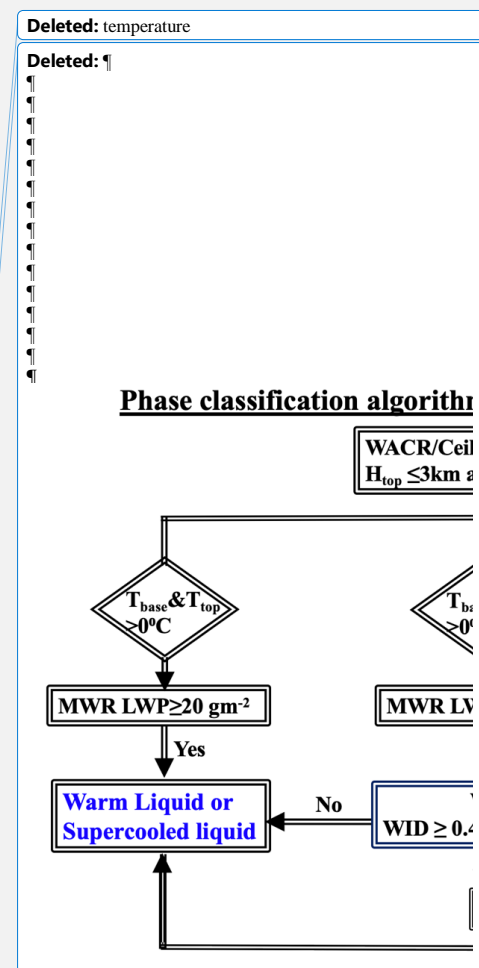


Figure 4. (a) Cloud liquid water paths (*LWPs*) retrieved from microwave radiometer (MWR) measured brightness [temperatures](#) using a physical retrieval method for each type of cloud. (b) The occurrence frequencies of $LWPs > 10 \text{ gm}^{-2}$ for each type of clouds



Phase classification algorithm for single layered low level clouds

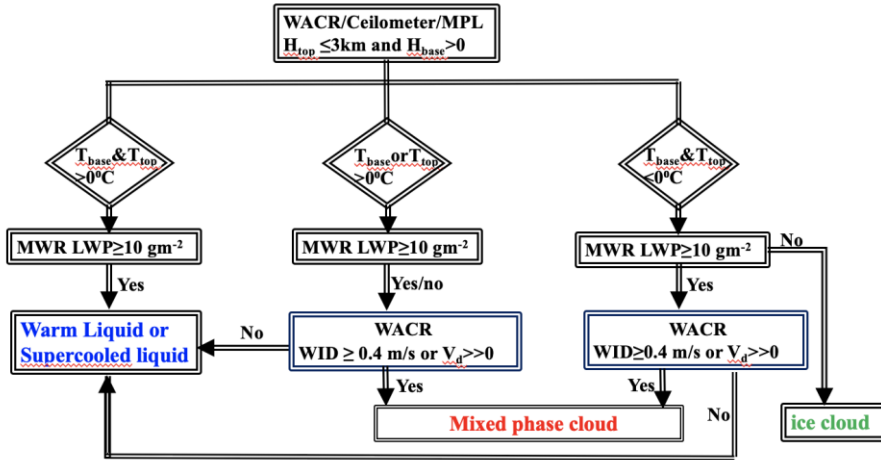
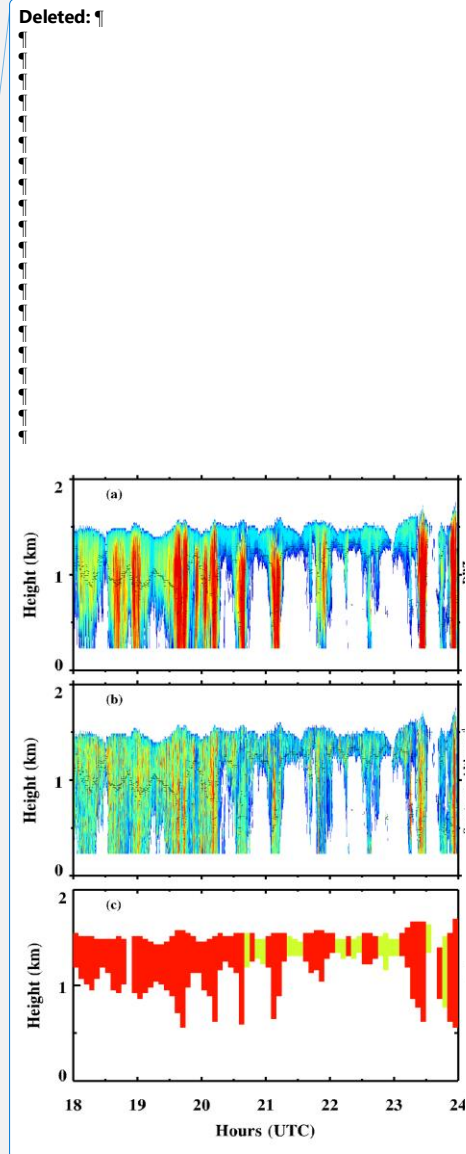


Figure 5. A flow chart for phase classification of single-layered low-level clouds. W-Band (95 GHz) ARM Cloud Radar (WACR) provides radar spectrum width (WID) and Doppler velocity (V_d).



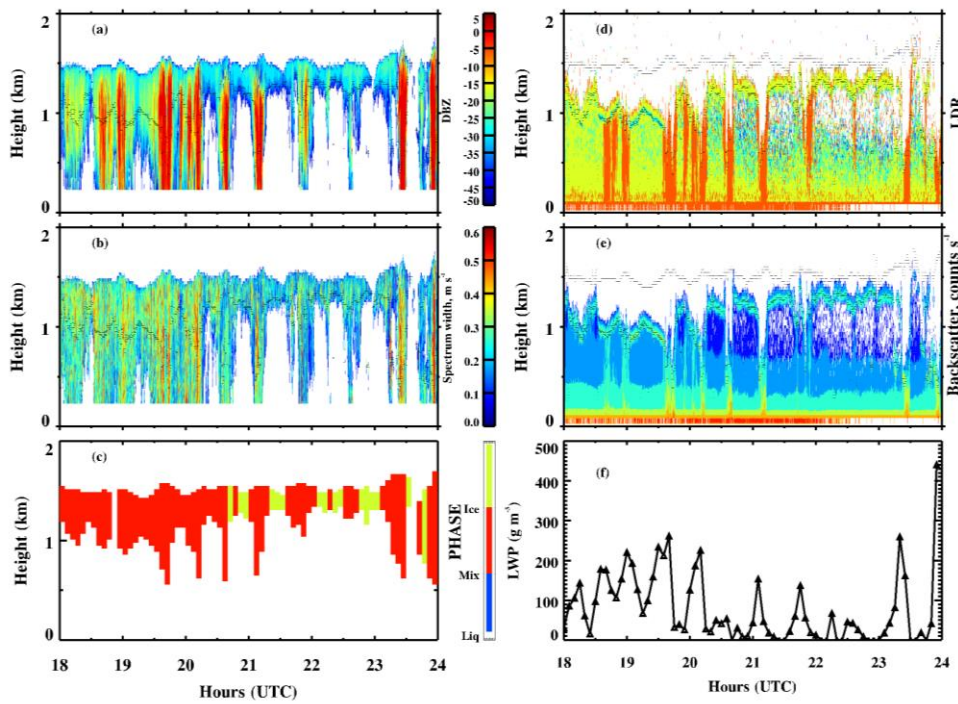
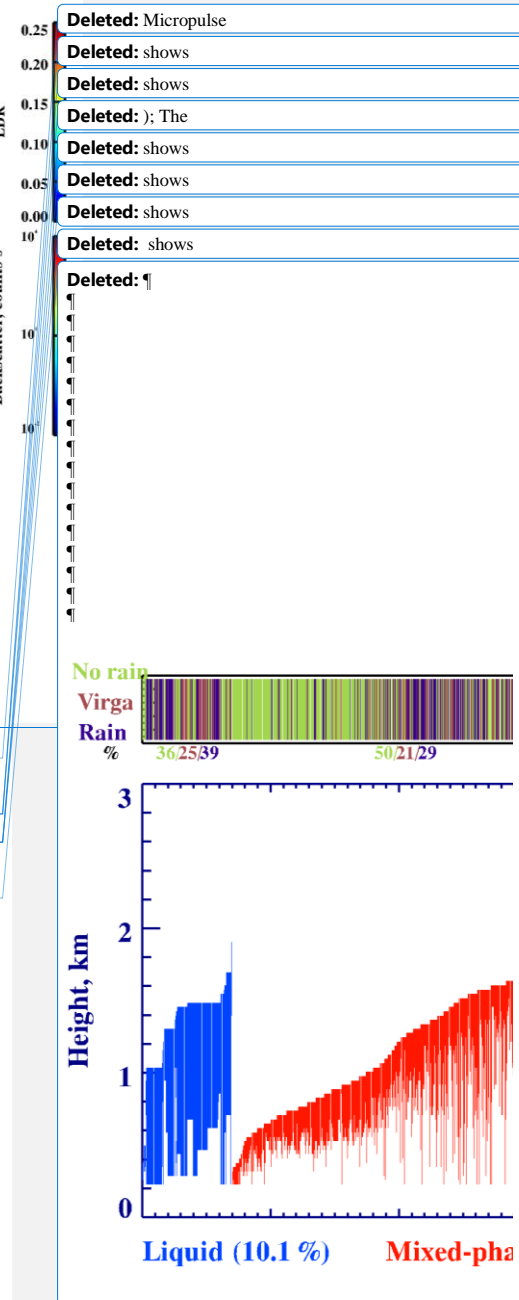


Figure 6. A case study that shows our phase classification (left column) and [MicroPulse Lidar \(MPL\)](#) linear depolarization ratios (*LDR*) and backscatter. W-Band (95 GHz) ARM Cloud Radar (WACR) reflectivity [is shown](#) in (a) and spectrum width [is shown](#) in (b). [Correspondingly, the phase classification is shown](#) in (c); MPL *LDR* in (d) and backscatter in (e); and [MWR-derived LWP](#) in (f).



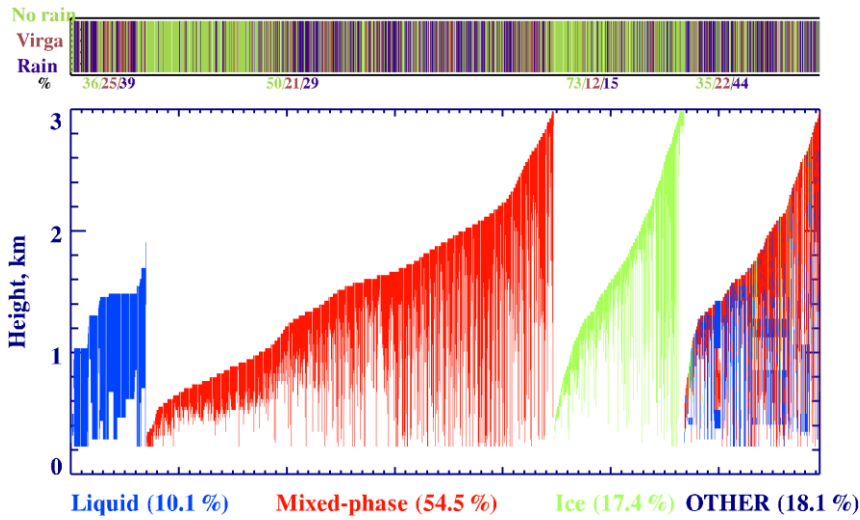


Figure 7. (Upper Panel) The drizzling status for each categorized cloud type, e.g., no rain (yellow-green), virga (brown) and rain (navy blue), the percentages shown below the x-axis represent the portion of drizzling in each type of clouds. (Bottom Panel) The percentages and vertical distributions of classified liquid, mixed-phase, ice, and 'OTHER' clouds for each column in the single-layered low-level clouds, represented by different colors, over the entire domain during MARCUS. Each line represents one 5-min sample. [The definition of drizzle here is the radar reflectivity below the ceilometer-derived cloud base, which could be either liquid drizzle drops or ice crystals.](#)

Deleted: ; And

Deleted: the

Deleted: ¶

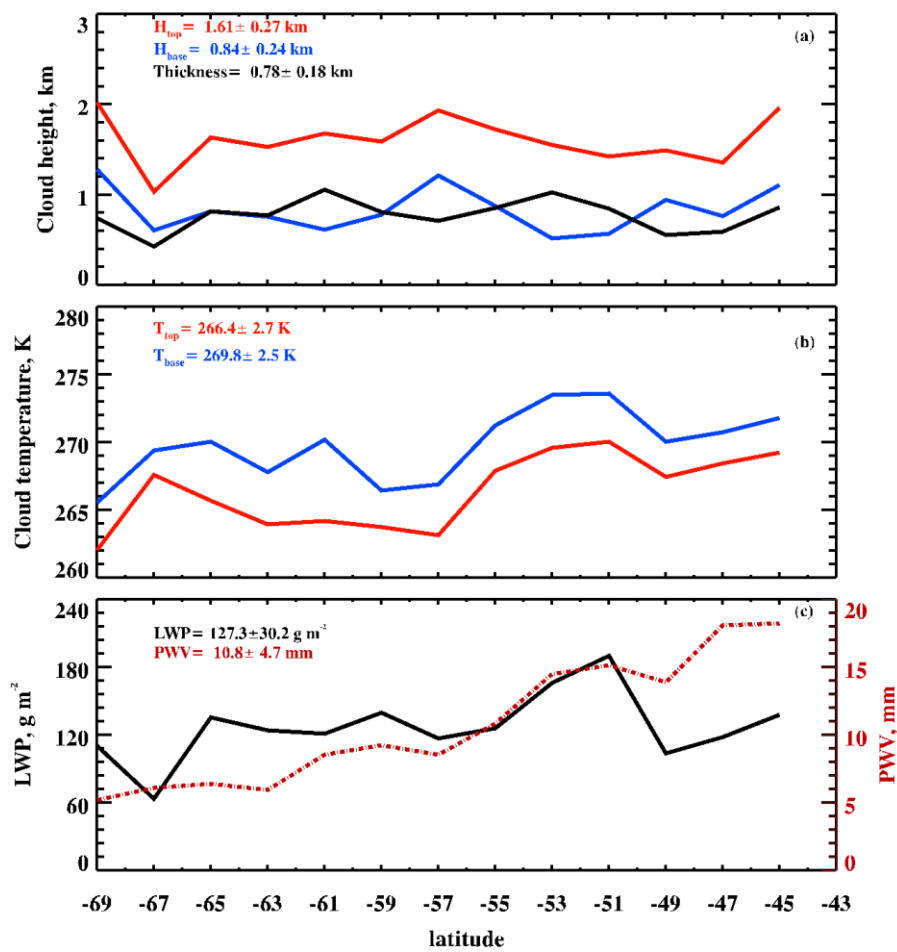
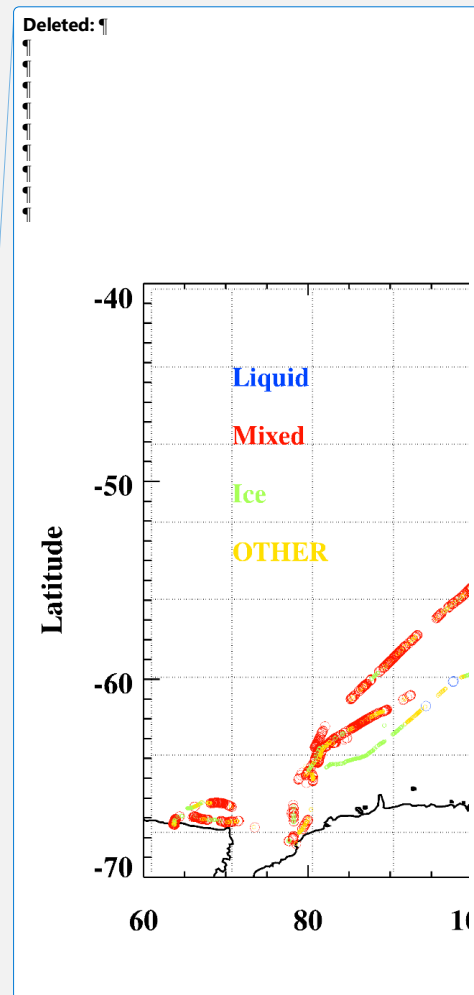


Figure 8. Meridional variations of single-layered low-level cloud properties: (a) cloud-base (H_{base}) and -top (H_{top}) heights, and cloud thickness (ΔH), (b) cloud-base (T_{base}) and -top (T_{top}) temperatures, and (c) cloud liquid water path (LWP) and precipitable water vapor (PWV) over the entire domain during MARCUS.



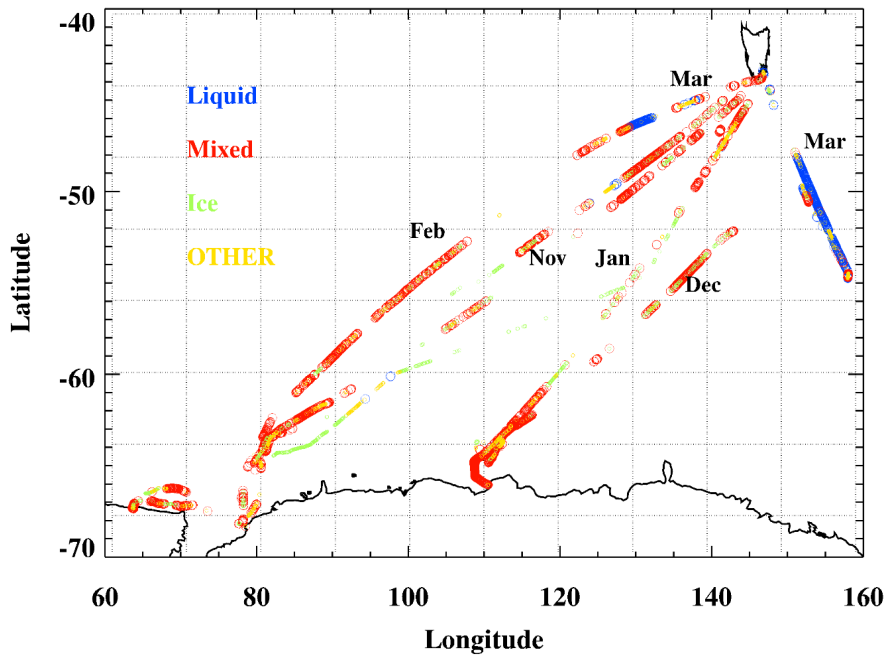
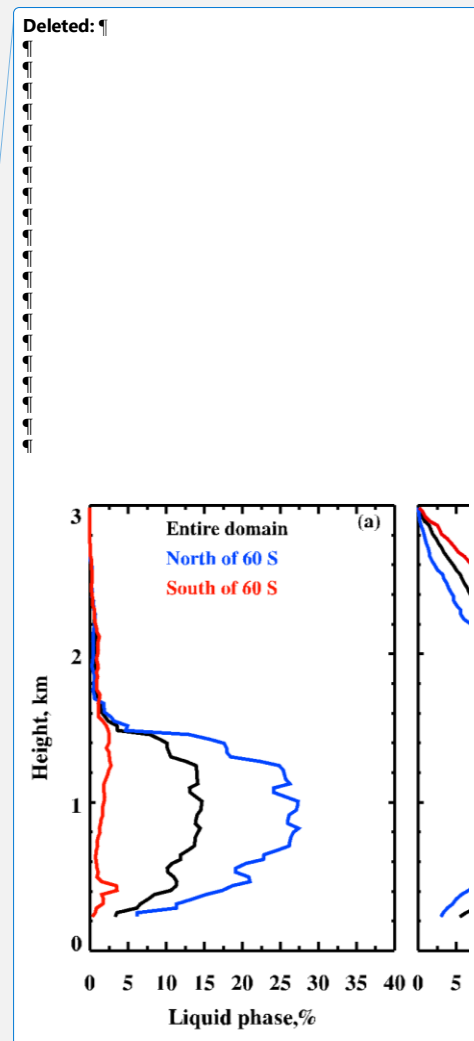


Figure 9. The latitudinal and longitudinal distributions of classified mixed-phase, liquid, and ice clouds in the single-layered low-level clouds. The liquid (blue), mixed (red), ice (light green), and OTHER (yellow) are shown along each shiptrack from October 2017 to March 2018 during MARCUS.



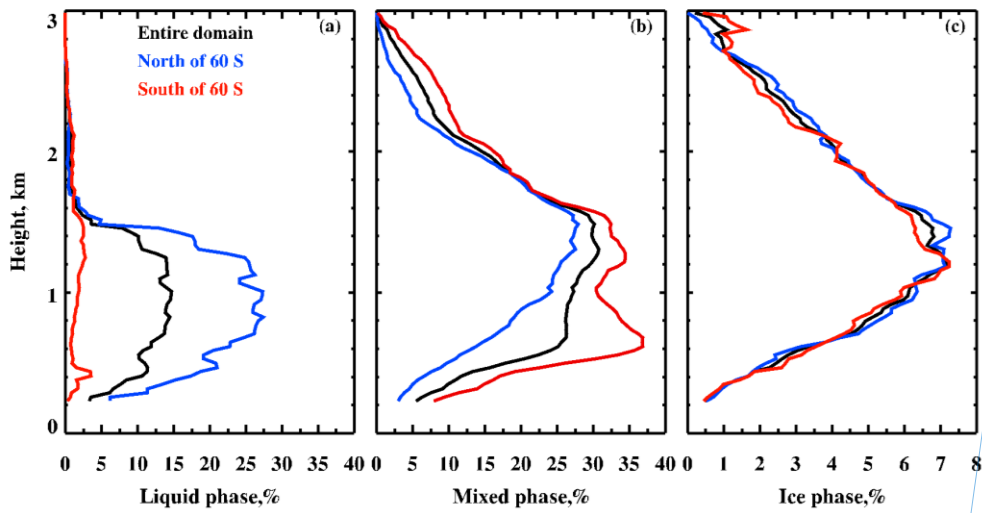
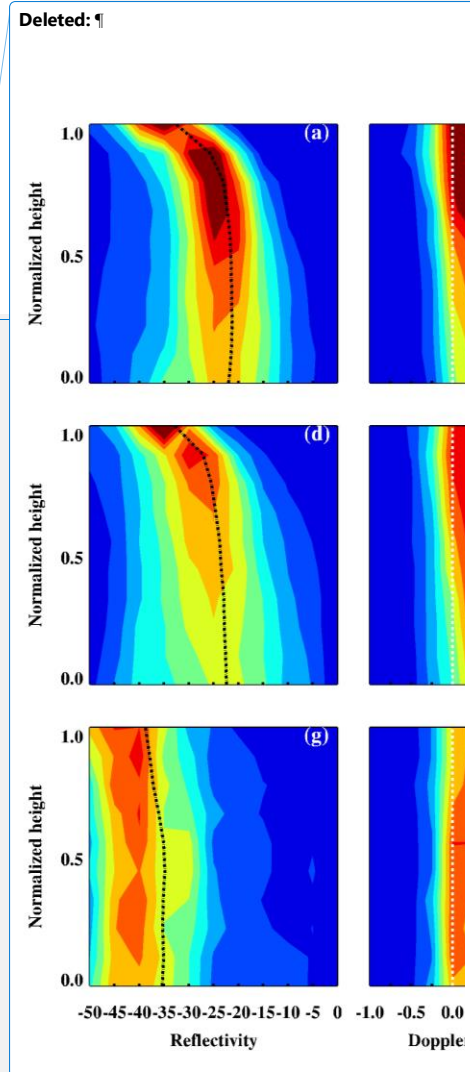


Figure 10. Occurrence frequencies of classified mixed-phase, liquid, and ice clouds over the entire domain (black), North of 60°S (blue) and South of 60°S (red) during MARCUS.



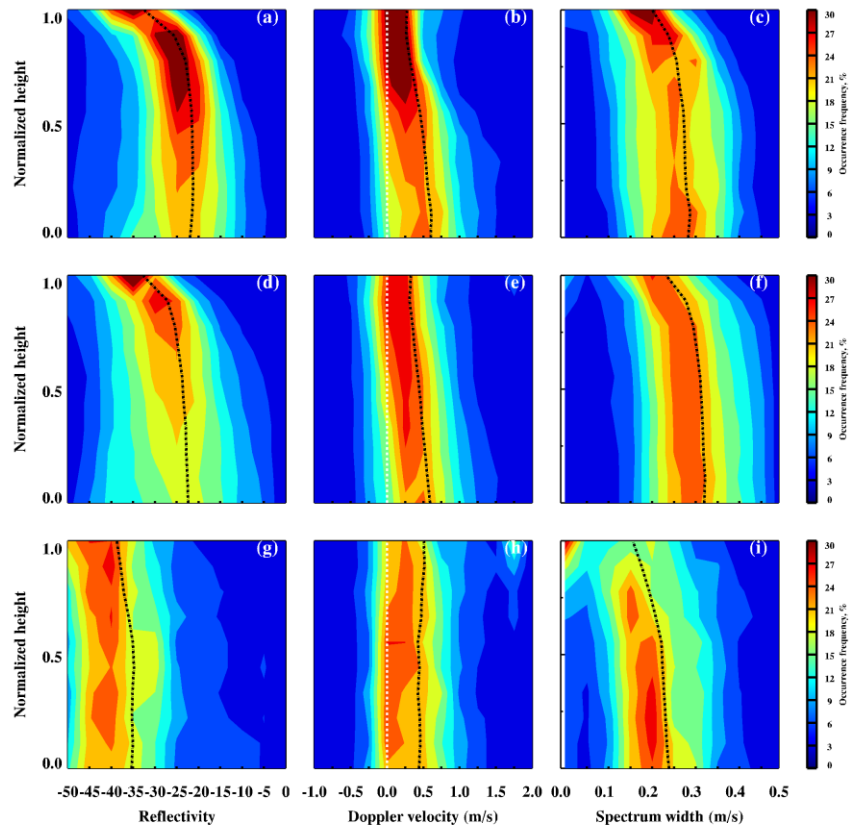


Figure 11. Normalized vertical distributions of radar reflectivity (a), Doppler velocity (b) and spectrum width (c) for the classified liquid (upper panel), mixed-phase (d to f, middle panel) and ice (g to i, bottom panel) clouds over the North of 60°S during MARCUS Intensive observational period (IOP). Normalized height is defined as $\frac{H-H_{base}}{H_{top}-H_{base}}$ where cloud base is denoted as 0 and cloud top is 1. The black lines represent the median values and the white lines in Doppler velocity represent the reference of 0.0 m s⁻¹.

Deleted: a)

Deleted: , b)

Deleted: c)

Deleted: IOP.

Deleted: ¶

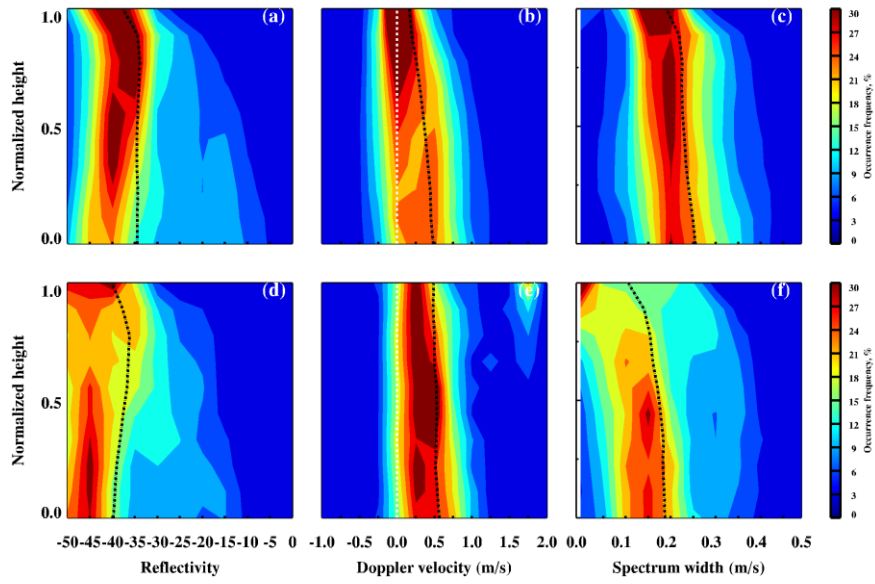


Figure 12. Same as Fig. 11 but only for mixed-phase (a to c, upper panel) and ice (d to f, bottom panel) over the south of 60°S during MARCUS.

Deleted: ¶